Università degli Studi di Padova

Facoltà di Scienze MM.FF.NN.

Anno Accademico 2013/2014

Tesi di Laurea Magistrale in Fisica

Study of variational symplectic algorithms for the numerical integration of guiding center equations of motion.

Relatore: Dr. Fabio Sattin
Correlatore: Prof. Luca Salasnich

Laureando: Filippo Zonta

Contents

1 Guiding Center Integrators: Numerical Results

1.1 Introduction

In the last chapter, we studied the behaviour of a variational symplectic integrator when applied to a phase-space Lagrangian.
In particular, we proved that its flow is in general splitted in two parts each of which admits a continuous limit.
Particular attention must be paid to the conservation of the continuous constraints. In this regard, we saw that for a Hamiltonian system with a constant symplectic form, such as canonical systems, the constraints are conserved and a good projection can be defined, such that it is symplectic and consistent woth the original continuous problem.
The same simple arguments do not hold for a non constant symplectic form: the Taylor expansion made in eqs.(**??**) doesn't stop at the first terms and additional terms with the same sign arise. Hence, equation (**??**) does not hold and the constraints $\phi_k = \Theta_k - p_k$ are not conserved and it is not possible to define a trivial projection to the submanifold M.
However, we will see that the integrator does still possess good long-term conservation properties. The reason of this behaviour is still unknown.
It is possible that non trivial quantities dependent on the time step h are conserved by each part of the splitted flow.

In this chapter, we will study the variational symplectic integrator applied to the non canonical guiding center theory.
We will follow the guidelines given by Qin and coworkers in a series of paper ([19] and [20]), where different versions of the integrator were studied, in particular an explicit linearization of the flow.
We want to anticipate here that all the integrators are very sensible to the initial conditions, and it is not clear at the moment which is the best choice of initialization, given a particular choice of the algorithm.
The complete understanding of the theory underlying these types of integrators for non constant symplectic forms is of great importance, since it can lead to better choice of initial conditions and possibly to new versions of the algorithm.

Let's start by recalling some basic results of the non canonical guiding center theory of chapter **??**.
The guiding center Hamiltonian one-form and symplectic form are given by:

$$\Theta = \begin{pmatrix} \mathbf{A}^\dagger \\ 0 \end{pmatrix}$$

$$\Omega = \begin{pmatrix} 0 & -B_z^\dagger & B_y^\dagger & \hat{b}_x \\ B_z^\dagger & 0 & -B_x^\dagger & \hat{b}_y \\ -B_y^\dagger & B_x^\dagger & 0 & \hat{b}_z \\ -\hat{b}_x & -\hat{b}_y & -\hat{b}_z & 0 \end{pmatrix}$$

where $A^\dagger$ and $B^\dagger$ are respectively the modified vector potential and the modified magnetic field:

$$\mathbf{A}^\dagger(\mathbf{X}, t) = \mathbf{A}(\mathbf{X}, t) + u\hat{\mathbf{b}}(\mathbf{X}, t) \tag{1.1a}$$

$$\mathbf{B}^\dagger = \nabla \times \mathbf{A}^\dagger = \mathbf{B} + u\nabla \times \hat{\mathbf{b}} \tag{1.1b}$$

The resulting phase-space Lagrangian is given by:

$$\begin{aligned} \mathcal{L}(\mathbf{x}, u, \dot{\mathbf{x}}, \dot{u}) &= \Theta(\mathbf{x}, u) \cdot (\dot{\mathbf{x}}, \dot{u}) - H(\mathbf{x}, u) \\ &= A^\dagger \cdot \dot{\mathbf{x}} - H(\mathbf{x}, u) \end{aligned} \tag{1.2}$$

where $H(\mathbf{x}, u)$ is the non canonical Hamiltonian:

$$H(\mathbf{x}, u) = \frac{u^2}{2} + \mu B \tag{1.3}$$

The equations of motion read:

$$\begin{pmatrix} \dot{\mathbf{x}} \\ \dot{u} \end{pmatrix} = -\Omega(\mathbf{x}, u)^{-1} \nabla H(\mathbf{x}, u) \tag{1.4}$$

or equivalently:

$$\dot{\mathbf{X}} = \frac{u\mathbf{B}^\dagger - \hat{\mathbf{b}} \times (\mathbf{E} - \mu\nabla B)}{\hat{\mathbf{b}} \cdot \mathbf{B}^\dagger} \tag{1.5a}$$

$$\dot{u} = \frac{\mathbf{B}^\dagger \cdot (\mathbf{E} - \mu\nabla B)}{\hat{\mathbf{b}} \cdot \mathbf{B}^\dagger} \tag{1.5b}$$

With equations (1.5) we can easily build a standard, i.e. non symplectic, integrator, such as Euler or Runge-Kutta.
We can use these integrators as a direct comparison with the symplectic ones. Also, since they share the same degrees of freedom of the continuous system, they can be used to build an initialization starting from a point z_0.
Finally, they are useful as a first guess for the solution of the implicit equations of the variational integrator.

1.2 Magnetic Field Configurations

In this thesis, the variational integrators were tested with three different magnetic field configurations: a uniform magnetic field, a tokamak configuration and a force free magnetic field.

1.2.1 Reference Case A: Two Dimensional Uniform Magnetic Field

As a first example, we can choose a magnetic field directed along the z axis and dependent weakly on the other two variables:

$$\mathbf{A}(\mathbf{x}) = -\frac{0.05}{3}y^3\hat{\mathbf{e}}_x + \left(\frac{0.05}{12}x^3 + x\right)\hat{\mathbf{e}}_y \tag{1.6a}$$

$$\mathbf{B}(\mathbf{x}) = 1 + 0.05\left(\frac{x^2}{4} + y^2\right)\hat{\mathbf{e}}_z \tag{1.6b}$$

$$\tag{1.6c}$$

Since there is no dependence on the z axis, the third component of the modified vector field (see eq.1.2) is a conserved quantity:

$$\frac{\partial \mathcal{L}}{\partial \dot{z}} = A_z^\dagger = A_z + u\hat{b}_z = u = const. \tag{1.7}$$

One can easily show that, since the Lagrangian is independent from $\dot{u}$, we can reduce the system by substituting u with a particular solution, which in this case is just a constant.
Finally, the variable z appears in the Lagrangian only with a term $k\dot{z}$, so it can be safely dropped and we get the following reduced Lagrangian:

$$\mathcal{L}(x, y, \dot{x}, \dot{y}) = \begin{pmatrix} A_x \\ A_y \end{pmatrix} \cdot \begin{pmatrix} \dot{x} \\ \dot{y} \end{pmatrix} - \mu B(x, y) \tag{1.8}$$

Hence, the magnitude of the magnetic field along an orbit is conserved and the dynamics in the x-y plane is a closed orbit with equation:

$$\frac{x^2}{4} + y^2 = const \tag{1.9}$$

From the theory presented in chapter **??**, we expect that a symplectic integrator should conserve exactly the quantities associated with Noether symmetries, in this case the velocity u, while the magnitude of the magnetic field, which represents the energy, should possess good long time bounding properties.

Parameters We chose the time step such that the integrator completes one orbit in about 50 steps: $h \simeq \frac{T}{50}$, which turns out to be $h \simeq 1 \times 10^6$.
The initial position of the particle is chosen to be $\mathbf{x}_0 = (0.05, 0, 0)$ with an initial velocity $u_0 = 3.9 \times 10^{-4}$.

1.2.2 Reference Case B: Tokamak magnetic field

As a more complicated example, we can choose a typical magnetic field configuration used in tokamak fusion reactor. Denoting by z the toroidal coordinate and by x, y the coordinates of the poloidal plane, the vector potential and the magnetic field are:

$$A = -B_0 R_0 ln\left(\frac{R_0 + x}{R_0}\right)\hat{\mathbf{y}} + \frac{B_0}{2q(R_0 + x)}\left[2R_0(R_0 + x)ln\left(\frac{R_0 + x}{R_0}\right) - 2R_0 x - 2x^2 - y^2\right]\hat{\mathbf{z}} \tag{1.10a}$$

$$B = -\frac{B_0 y}{q(R_0 + x)}\hat{\mathbf{x}} + \frac{B_0}{q}\frac{2R_0 x + 2x^2 - y^2}{2(R_0 + x)^2}\hat{\mathbf{y}} - \frac{B_0 R_0}{R_0 + x}\hat{\mathbf{z}} \tag{1.10b}$$

In this case, the magnetic field is toroidally symmetric and its field lines are almost circular concentric in the poloidal plane, as illustrated in fig. 1.

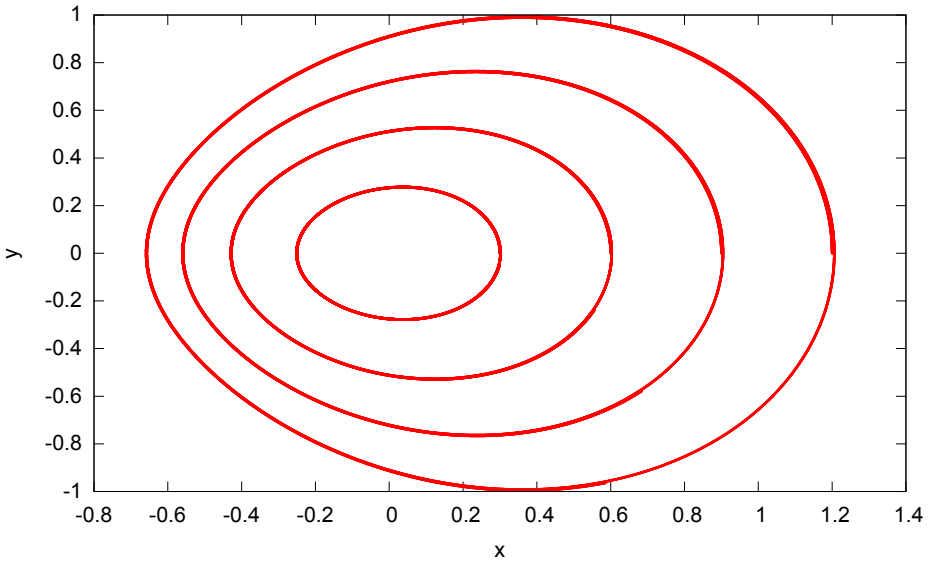

Figure 1: Magnetic field lines for the tokamak B configuration (section 1.2.2)

As before, the fact that the fields are toroidally symmetric implies that the relative conjugate momentum, which is the z-th component of the modified vector

potential, is a conserved quantity:

$$A_z^\dagger(\mathbf{x}, u) = A_z(\mathbf{x}) + u\hat{b}(\mathbf{x}) \tag{1.11}$$

The dynamics in the poloidal plane is a closed orbit which can be elliptic or a banana orbit if the energy of the particle is sufficiently low so that the parallel gradient drift is enough to bounce back the particle (see section **??**).

Parameters The magnetic field and the minor radius B_0, R_0 are chosen to be normalized to unity with a safety factor $q = 2$ and a magnetic moment of $\mu = 2.25 \times 10^{-6}$.
Using the same initial conditions of the configuration A, the particle performs banana orbits in the poloidal plane.
The time step used is $h = 800$ which corresponds to $h \simeq \frac{T}{50}$. Summing up:

h	800
R_0	1
B_0	1
q	2
μ	2.25×10^{-6}
$\mathbf{x}_0$	$(0.05, 0, 0)$
u_0	3.9×10^{-4}

1.2.3 Reference Case C: force-free field

The equilibrium state of a plasma is described by the equilibrium of the magnetic and pressure forces:

$$\mathbf{J} \times \mathbf{B} = \nabla p \tag{1.12}$$

Also, the condition of null divergence of the magnetic field and the Ampere's law read:

$$0 = \nabla \cdot \mathbf{B} \tag{1.13a}$$

$$\mathbf{J} = \nabla \times \mathbf{B} \tag{1.13b}$$

When the kinetic pressure of a plasma is negligible, its magnetic field assumes the following form at equilibrium:

$$0 = \mathbf{J} \times \mathbf{B} = (\nabla \times \mathbf{B}) \times \mathbf{B} \tag{1.14}$$

hence, the curl of the magnetic field must be parallel to the field:

$$\nabla \times \mathbf{B} = a\mathbf{B} \tag{1.15}$$

where a is a parameter that can depend in principle on the space. These types of magnetic field are called force-free and they are of particular importance in astrophysics and in the RFP fusion reactor, where the condition on the kinetc pressure is almost satisfied.
In our case we assume the parameter a to be constant. The magnetic field in this case is said to be linear force-free.

The solution of equation (1.15) was first given by Namikawa [25] and Chandrasekhar [5].
Using the fact that the magnetic field has null divergence, we can express eq.(1.14) as:

$$\nabla^2 \mathbf{B} + a^2 \mathbf{B} = 0 \tag{1.16}$$

which is the vector Helmholtz equation. It was proved by Chandrasekhar and Namikawa that given a solution ψ of the scalar Helmholtz equation:

$$\nabla^2 \psi + a^2 \psi = 0 \tag{1.17}$$

then a solution in cylindrical coordinates (r, θ, z) of the force-free equation (1.15) can be found with:

$$\mathbf{B} = \frac{1}{\mu} \nabla \times (\nabla \times \hat{\mathbf{z}} \psi) + \nabla \times \hat{\mathbf{z}} \psi \tag{1.18}$$

The corresponding vector field is then:

$$\mathbf{A} = \frac{1}{a} \nabla \times \hat{\mathbf{z}} \psi + \hat{\mathbf{z}} \psi \tag{1.19}$$

Since we are assuming periodicity along the toroidal and polodial axes, we can express a generic solution in terms of the poloidal and toroidal numbers and it turns out that each term is just the Bessel function:

$$\psi(r, \theta, z) = \sum_{m,n} J_m \left(r a_n \right) e^{im\theta + inz} \tag{1.20a}$$

$$a_n = \sqrt{a^2 - n^2} \tag{1.20b}$$

Reference Case C1: Axial Symmetric field Using equation (1.18) we can find the first term $(n = 0, m = 0)$ in expansion (1.20):

$$\mathbf{B}_{00}(r, \theta, z) = B_0 J_1(ar) \hat{\mathbf{e}}_\theta + B_0 J_0(ar) \hat{\mathbf{e}}_z \tag{1.21}$$

the vector potential is:

$$\mathbf{A}_{00}(r,\theta,z) = \frac{B_0}{a} J_1(ar)\hat{\mathbf{e}}_\theta + \frac{B_0}{a} J_0(ar)\hat{\mathbf{e}}_z \tag{1.22}$$

As illustrated in figure 2, the toroidal magnetic field is inverted at a specific radius point, that is $ar \simeq 2.4$. This is a typical behaviour found in the RFP experiments. Similarly to the tokamak configuration, when the energy of the particle is sufficiently low the dynamics in the poloidal plane is a closed banana orbit.

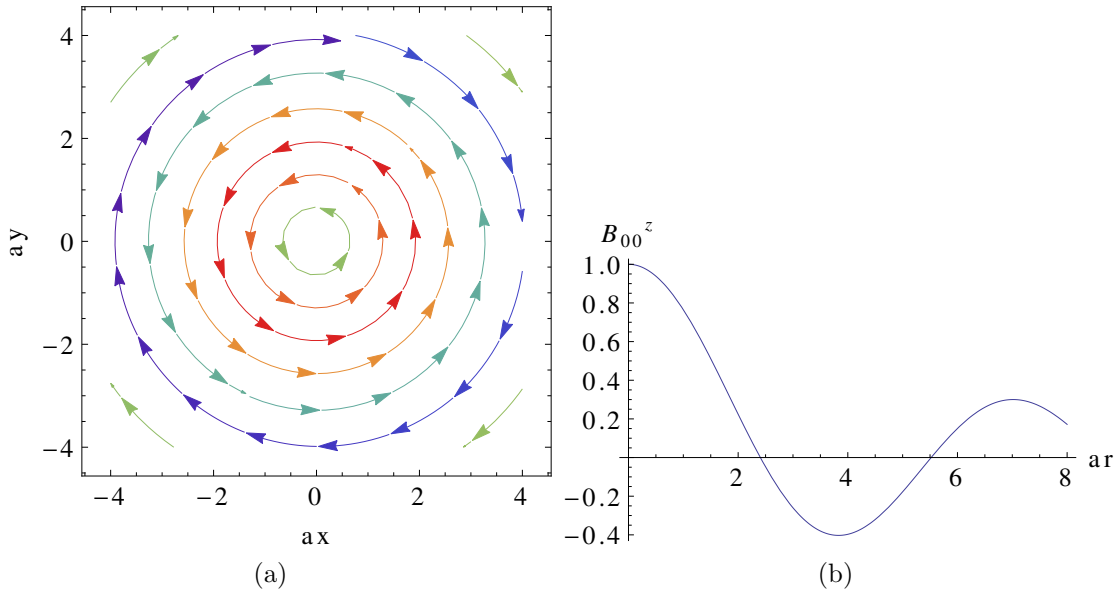

Figure 2: Field lines in the poloidal plane (a) and in the (z,r) plane (b) of the magnetic field configuration C1

Reference Case C2: Asymmetric field We tried a slightly more sophisticated configuration by adding small perturbations with numbers $(n = 1, m = 1)$ and $(n = 1, m = 2)$:

$$\mathbf{B}(r,\theta,z) = \mathbf{B}_{00}(r,\theta,z) + \alpha\mathbf{B}_{11}(r,\theta,z) + \beta\mathbf{B}_{12}(r,\theta,z) \tag{1.23}$$

where $\mathbf{B}_{11}$ and $\mathbf{B}_{12}$ are found to be:

$$\begin{aligned}\mathbf{B}_{11}(r,\theta,z) = &\left[\frac{a_1}{a}J_0(a_1 r) + \frac{a-1}{ar}J_1(a_1 r)sin(\theta+z)\right]\hat{\mathbf{e}}_r \\ &+ \left[-a_{11}J_0(a_1 r) + \frac{a-1}{ar}J_1(a_1 r)cos(\theta+z)\right]\hat{\mathbf{e}}_\theta \\ &+ \left[\frac{a^2-1}{a}J_1(a_1 r)cos(\theta+z)\right]\hat{\mathbf{e}}_z\end{aligned} \tag{1.24}$$

$$\begin{aligned}\mathbf{B}_{12}(r,\theta,z) = &\left[\frac{2a_2}{a}J_0(a_2 r) + \frac{a-2}{ar}J_1(a_2 r)sin(\theta+2z)\right]\hat{\mathbf{e}}_r \\ &+ \left[-a_{12}J_0(a_2 r) + \frac{a-2}{ar}J_1(a_2 r)\right]cos(\theta+2z)\hat{\mathbf{e}}_\theta \\ &+ \left[\frac{a_2}{a}J_1(a_2 r)cos(\theta+2z)\right]\hat{\mathbf{e}}_z\end{aligned} \tag{1.25}$$

Note that the condition on the coefficients (1.20b) requires that the constant a must be greater than 2 for the perturbations to exist.
The effect of the perturbations on the field lines is plotted in fig. (3).
Note that we don't expect anymore closed orbits in the poloidal plane since the magnetic field is not perfectly symmetric along the toroidal axis.

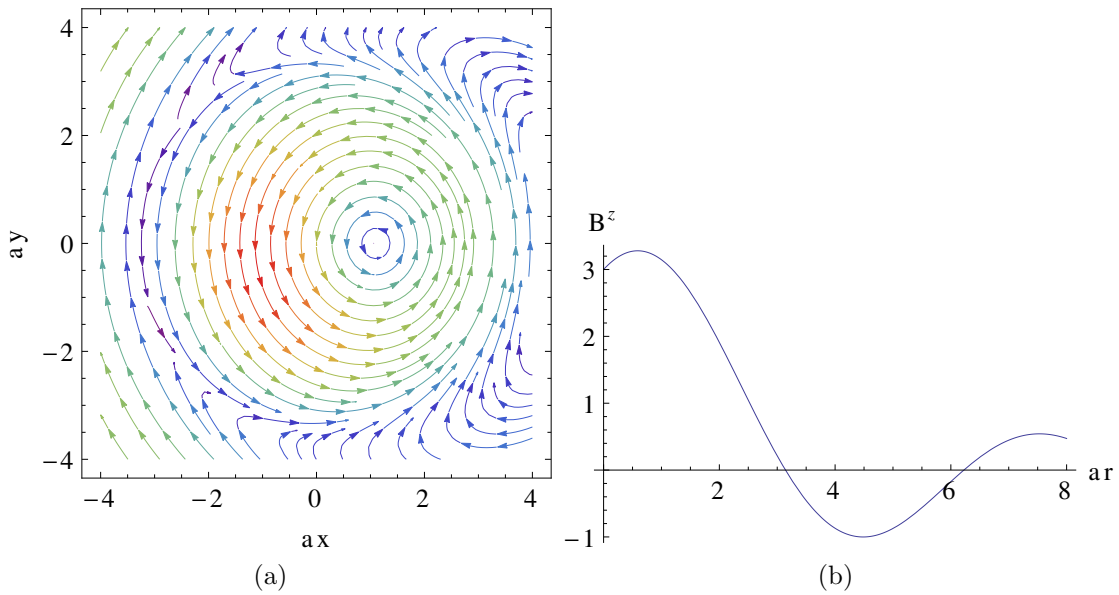

Figure 3: Field lines in the poloidal plane (a) and in the (z,r) plane (b) of the magnetic field configuration C2

Parameters We chose the parameter a to be $a = 3$, which leads to a typical RFP configuration. The radius r is assumed to be normalized to the minor radius of the reactor.
The velocity of the particle is selected to produce elliptic orbits for the symmetric version and banana orbits for the perturbed version.
The time step h corresponds to $h \simeq \frac{T}{50}$, where T is the period of the orbit.

h (C1)	240
h (C2)	600
a	3
$\mathbf{x}_0$	$(0.05, 0, 0)$
u_0 (C1)	3.9×10^{-4}
u_0 (C2)	3.9×10^{-5}
α	0.01
β	0.01

1.3 Initialization

As we will see, the choice of the initial points plays an important role, since different initializations, as we already saw in the last chapter, can lead to very different flows. In the following, we will use two different initializations.

Denoting by $\mathbf{z} = (\mathbf{x}, u)$ the coordinates of the phase-space, recall from section **??** that for a variational integrator we can study two different flows: the Lagrangian flow $(\mathbf{z}_0, \mathbf{z}_1) \to (\mathbf{z}_1, \mathbf{z}_2)$ and the hamiltonian flow $(\mathbf{z}_0, \mathbf{p}_0) \to (\mathbf{z}_1, \mathbf{p}_1)$.
Hence, this two flows induce two natural initializations: we call them Hamiltonian and Lagrangian initialization:

- **Hamiltonian Initialization**: given an initial point $\mathbf{z}_0$, $\mathbf{p}_0$ is selected by imposing the constraints:

$$\phi_0 = \mathbf{p}_0 - \frac{\partial \mathcal{L}}{\partial \dot{\mathbf{z}}} = \mathbf{p}_0 - \Theta_0 = \mathbf{p}_0 - \begin{pmatrix} A^\dagger(\mathbf{x}_0) \\ 0 \end{pmatrix} \equiv 0 \tag{1.26}$$

- **Lagrangian Initialization**: given an initial point $\mathbf{z}_0$, $\mathbf{z}_1$ is selected by evolving the continuous system to $\mathbf{z}_1$.
  In practice, an additional integrator, such as RK4, must be used. Of course, the point $\mathbf{z}_1$ can be find with arbitrary precision, for example by choosing small timesteps of the auxiliary integrator.

We recall that the initial points $\mathbf{z}_1$ and $\mathbf{p}_0$ are related by the left Legendre transform (see paragraph. **??**).

It makes sense, for the reasons we saw in the last chapter, that the Hamiltonian initialization can be the most correct one, since it guarantees that the flow is close to the continuous one for at least one time step and for the fact that it produces the correct result for the case of constant symplectic forms.
However, we will see that this is not always the case.

1.4 Numerical Schemes and Results

In the following, the continuous phase-space Lagrangian (eq. 1.2) was discretized with different methods: the midpoint rule, which produces generally the best results, a slightly modified version along with an explicit linearization, both suggested by Qin [19] and a midpoint discretization applied to a reduced Lagrangian.
Finally, new explicit linearizations are proposed and we will show some interesting benefits over the old algorithms.

For now on, we will refer to z^i as the coordinates of the phase-space

$$\mathbf{z} = (\mathbf{x}, u) \tag{1.27}$$

and to $\tilde{z}$ and Δz as the midpoint discretization of $\mathbf{z}$ and $\dot{\mathbf{z}}$:

$$\begin{aligned} \tilde{\mathbf{z}}_k &= \frac{\mathbf{z}_k + \mathbf{z}_{k+1}}{2} \\ \Delta \mathbf{z}_k &= \mathbf{z}_{k+1} - \mathbf{z}_k \end{aligned} \tag{1.28}$$

Also, by $f_{i,j}$ we denote the derivative of the i-th component of the function f with respect to the j-th component:

$$f_{i,j}(\mathbf{z}) = \frac{\partial f_i(z)}{\partial \mathbf{z}_j} \tag{1.29}$$

Energy error Every integrator was tested by checking the conservation of the energy: denoting by H_0 and by H_k the hamiltonian evaluated at the time step 0 and k, the energy error is defined as:

$$\frac{dE}{E_0} = \frac{H_k - H_0}{H_0} \tag{1.30}$$

1.4.1 Implicit Scheme 1: Midpoint Rule

The discretization of the guiding center Lagrangian (1.2) with the midpoint rule (see eq.**??**) leads to the following expression:

$$\mathcal{L}_d(\mathbf{z}_0, \mathbf{z}_1) = A^\dagger(\tilde{\mathbf{z}}_0) \cdot \Delta\mathbf{x}_0 - h\mu B(\tilde{\mathbf{x}}_0) - h\frac{\tilde{u}_0^2}{2} \tag{1.31}$$

Recall from eq. (**??**) that the left and right discrete Legendre transforms for the midpoint rule are:

$$\begin{aligned} \mathbf{p}_k &= \frac{\partial \mathcal{L}}{\partial \dot{\mathbf{z}}}\left(\tilde{\mathbf{z}_k}, \frac{\Delta\mathbf{z}_k}{2}\right) - \frac{h}{2}\frac{\partial \mathcal{L}}{\partial \mathbf{z}}\left(\tilde{\mathbf{z}_k}, \frac{\Delta\mathbf{z}_k}{2}\right) \\ \mathbf{p}_{k+1} &= \frac{\partial \mathcal{L}}{\partial \dot{\mathbf{z}}}\left(\tilde{\mathbf{z}_k}, \frac{\Delta\mathbf{z}_k}{2}\right) + \frac{h}{2}\frac{\partial \mathcal{L}}{\partial \mathbf{z}}\left(\tilde{\mathbf{z}_k}, \frac{\Delta\mathbf{z}_k}{2}\right) \end{aligned} \tag{1.32}$$

For the guiding center we get the following expressions:

$$\mathbf{p}_0^{\mathbf{x}} = -\frac{1}{2}\left(A^\dagger_{i,j}(\tilde{\mathbf{x}}_0)\right) \cdot (\Delta\mathbf{x}_0) + A^\dagger_j(\tilde{\mathbf{x}}_0) + \frac{h}{2}\mu B_{,j}(\tilde{\mathbf{x}}_0) \tag{1.33a}$$

$$p_0^u = -\frac{1}{2}\hat{b}(\tilde{\mathbf{x}_0}) \cdot (\Delta\mathbf{x}_0) + \frac{h}{2}\tilde{u}_0 \tag{1.33b}$$

$$\mathbf{p}_1^{\mathbf{x}} = \frac{1}{2}\left(A^\dagger_{i,j}(\tilde{\mathbf{x}}_0)\right) \cdot (\Delta\mathbf{x}_0) + A^\dagger_j(\tilde{\mathbf{x}}_0) - \frac{h}{2}\mu B_{,j}(\tilde{\mathbf{x}}_0) \tag{1.33c}$$

$$p_1^u = \frac{1}{2}\hat{b}(\tilde{\mathbf{x}_0}) \cdot (\Delta\mathbf{x}_0) - \frac{h}{2}\tilde{u}_0 \tag{1.33d}$$

Given an initial points $\mathbf{x}_0, u_0, p_0^{\mathbf{x}}, p_0^p$, the first two equations of (1.33) are inverted to find the points $\mathbf{x}_1, u_1$ and the momenta $p_1^{\mathbf{x}}, p_1^p$ are found with the last two equations. Of course, this is a way to compute the Hamiltonian flow.

It is equivalent to start with two points $\mathbf{x}_0, u_0, \mathbf{x}_1, u_1$ and find $\mathbf{x}_2, u_2$ by matching the momenta of eqs (1.33):

$$\frac{1}{2}\left(A^\dagger_{i,j}(\tilde{\mathbf{x}}_0)\right) \cdot (\Delta\mathbf{x}_0) + \frac{1}{2}\left(A^\dagger_{i,j}(\tilde{\mathbf{x}}_1)\right) \cdot (\Delta\mathbf{x}_1) + A^\dagger_j(\tilde{\mathbf{x}}_0) - A^\dagger_j(\tilde{\mathbf{x}}_1) - \frac{h}{2}\mu\left[B_{,j}(\tilde{\mathbf{x}}_0) + B_{,j}(\tilde{\mathbf{x}}_1)\right] = 0 \tag{1.34a}$$

$$\frac{1}{2}\hat{b}(\tilde{\mathbf{x}_0}) \cdot (\Delta\mathbf{x}_0) + \frac{1}{2}\hat{b}(\tilde{\mathbf{x}_1}) \cdot (\Delta\mathbf{x}_1) - \frac{h}{2}(u_2 + 2u_1 + u_0) = 0 \tag{1.34b}$$

In either way, the resolution of the flow requires the inversion of an implicit equation.
This is done by using an auxiliary integrator, in our case RK4 applied to the continuous equations of motion (**??**), and by converging to the implicit equations (1.33) with sufficiently high number of Newton iterations. Usually, three or four iterations are enough to guarantee a good accuracy.

We expect for the field configurations A,B and C1, for which there is a translational symmetry along the z axis, that the correspondent discrete momentum is conserved by the integrator:

$$p_k^z = \frac{\partial \mathcal{L}}{\partial \dot{z}} \left(\tilde{\mathbf{z}_k}, \frac{\Delta \mathbf{z}_k}{2} \right) = A_z^\dagger(\tilde{\mathbf{x}}_k) = const. \tag{1.35}$$

Also, since the Lagrangian is independent from $\dot{u}$, we expect that the conjugate momentum of u is inverted at each step. In fact, from the definition of the discrete Legendre transforms (eqs. 1.32), we get:

$$p_k^u = -\frac{h}{2} \frac{\partial \mathcal{L}}{\partial u} \left(\tilde{\mathbf{z}_k}, \frac{\Delta \mathbf{z}_k}{2} \right) = -p_{k+1}^u \tag{1.36}$$

Of course, this is just a particular case of the previous chapter, where we considered constant symplectic forms, or equivalently linear Cartan one-forms Θ.
In particular, if we restrict to the Hamiltonian initialization, for which the constraints are imposed at the first step (see paragraph 1.3), we expect that p^u should be exactly conserved.

Initialization In section (1.3), we said that different initializations can lead to different results.
At a first time, the midpoint discretization was tested with a Lagrangian initialization, so that given a point z_0, the point z_1 was found with a RK4 integrator applied to the equations of motion (1.5) with a small time step in order to guarantee the best accuracy.
Figure 4 illustrates the results for a tokamak configuration B.
The energy error oscillates with increasing amplitude and it becomes very inaccurate even after few steps.
This bad behaviour is similar for the other field configurations and is shared by all the implicit schemes we tested. This agrees with the discussions of the previous chapter, where we proved that, at least with simple cases, the Hamiltonian initialization was the most correct one. Hence, in the following we'll focus only on the Hamiltonian initialization.

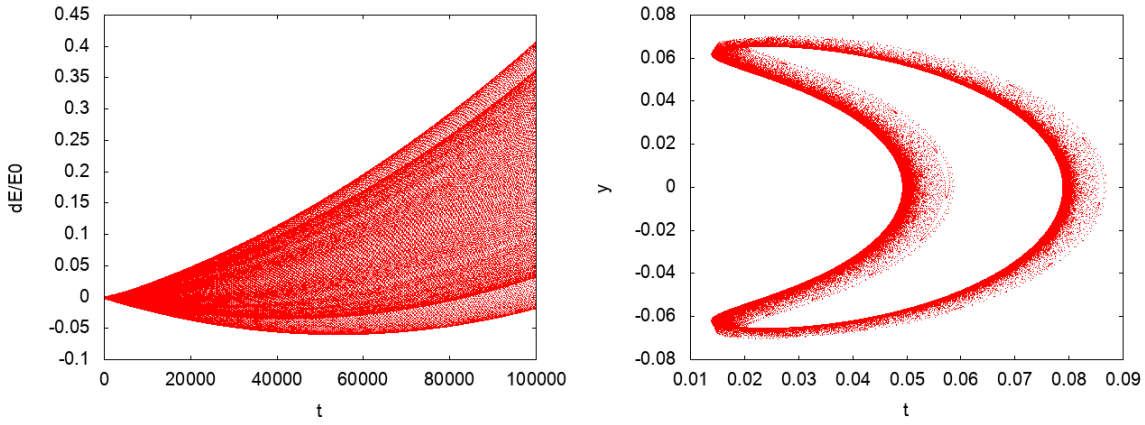

(a) (b)

Figure 4: Energy error (a) and particle orbit in the poloidal plane (b) for the midpoint rule with Lagrangian initialization applied to field configuration B.

Numerical Results Figure 5 shows the numerical results for the 2D field configuration A and the tokamak field B.
In both cases the momenta p_u and p_z are exactly conserved as expected. The energy is well bounded for long times, in particular for the configuration A the energy is exactly conserved.

For the tokamak field B we lowered the time step to $h = 10$ and plotted in figure 7 the conservation of the energy and the x component of the constraints:

$$\phi_x = p^x - A^{\dagger x} \tag{1.37}$$

We immediately notice that the constraint is not exactly conserved. As a consequence, the flow is splitted in two parts. The same behaviour happens for all the integrators we used in the rest of the thesis.

Unfortunately, the behaviour of the midpoint rule with the force-free fields C1 is slightly worse.
As shown in figure 8, the flow of the integrator is splitted in two parts with distinct energy.
While the momenta p^z and p^u are exactly conserved as expected, the energy of each part has a noticeable drift.

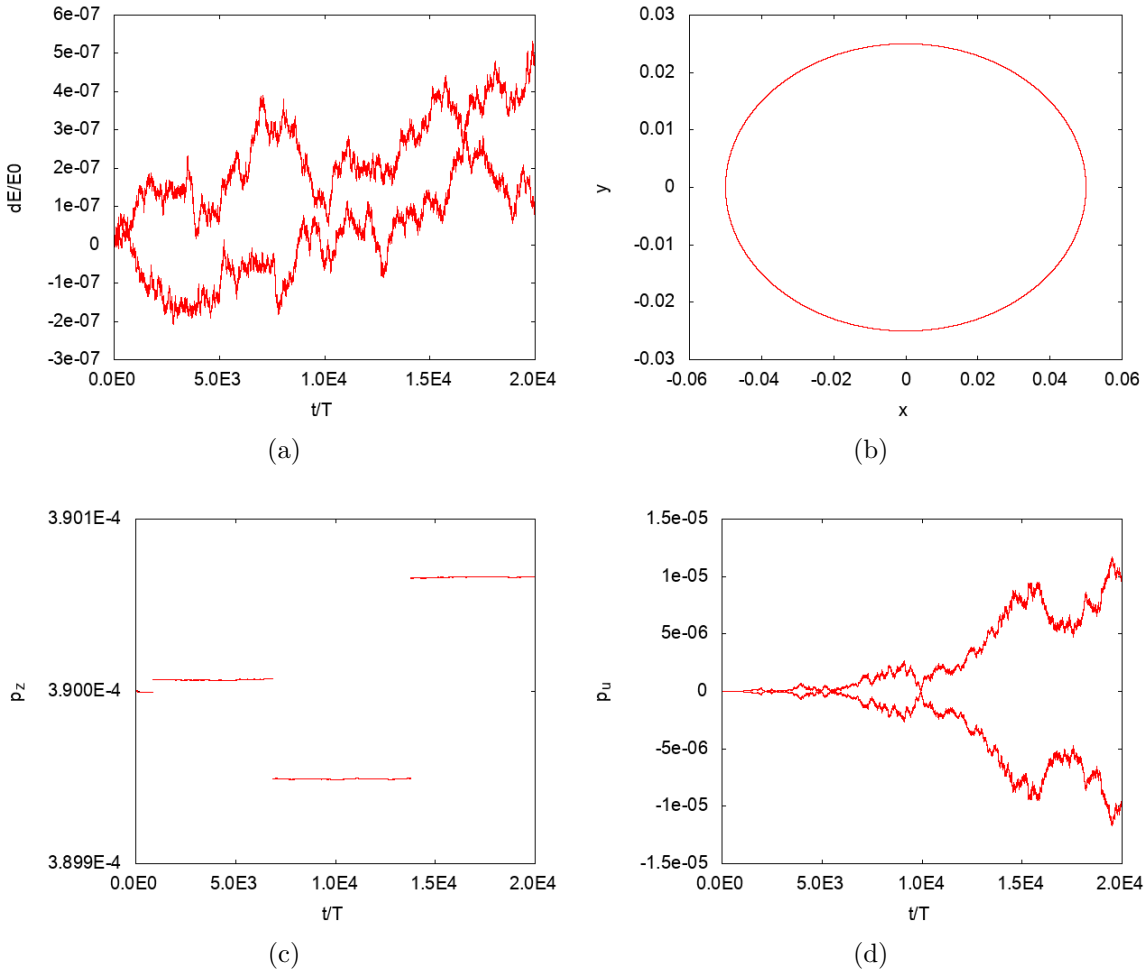

Figure 5: Midpoint rule applied to field configuration A. (a) is the energy error, (b) is the particle trajectory in the (x, y) plane, (c) and (d) are the z and u components of the discrete momentum (eq. 1.35)

For the configuration C2, the particle performs small banana orbits in the poloidal plane and a bigger elliptic closed orbit. The results are plotted in figure 9. A zoom of the trajectory with a low time step is reported in diagram (c) to highlight the banana orbits.
In this case, the energy is bounded correctly for long times and the momentum p^u is correctly conserved, while the momentum p^z is only bounded. This is expected, since the perturbations (eqs. 1.24) break the toroidal symmetry.

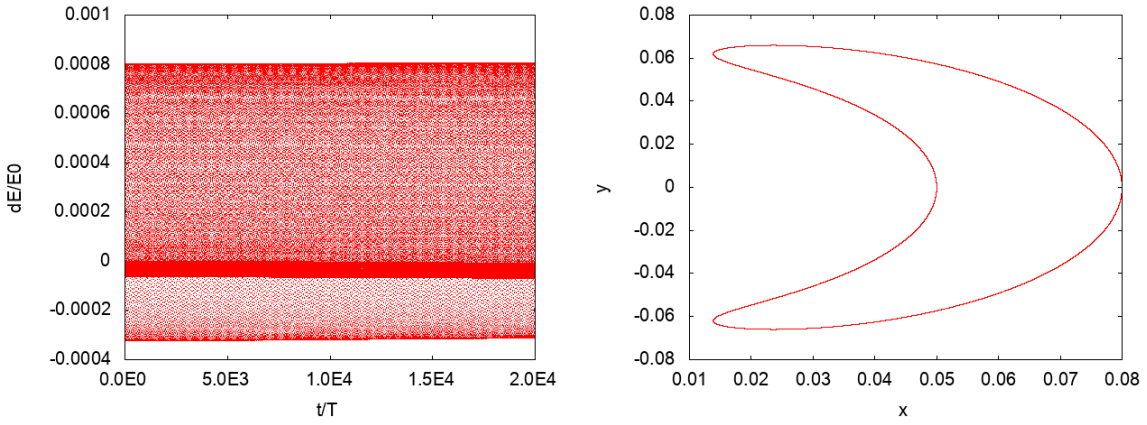

(a) (b)

(c) (d)

Figure 6: Midpoint rule applied to field configuration B. (a) is the energy error, (b) is the particle trajectory in the (x, y) plane, (c) and (d) are the z and u components of the discrete momentum (eq. 1.35)

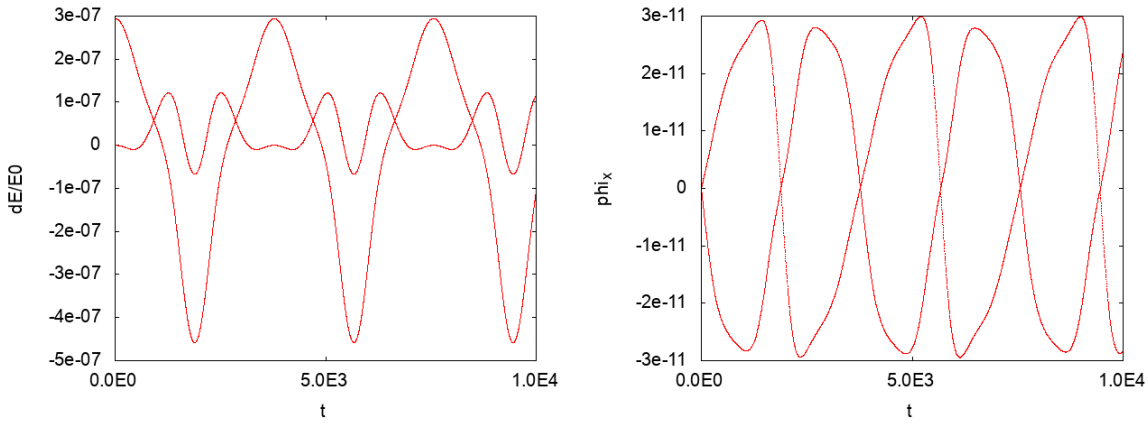

(a) (b)

Figure 7: Energy error (a) and x component of the constraints (eq. 1.37) (b) for the field configuration B with low time step ($h = 10$)

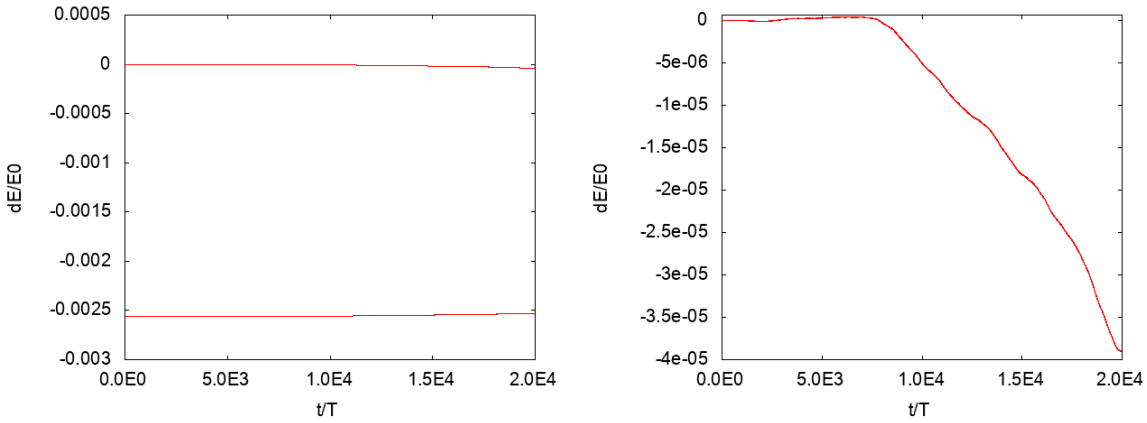

(a)

(b)

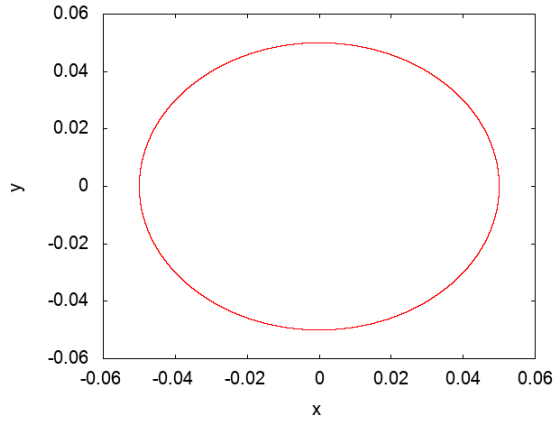

(c)

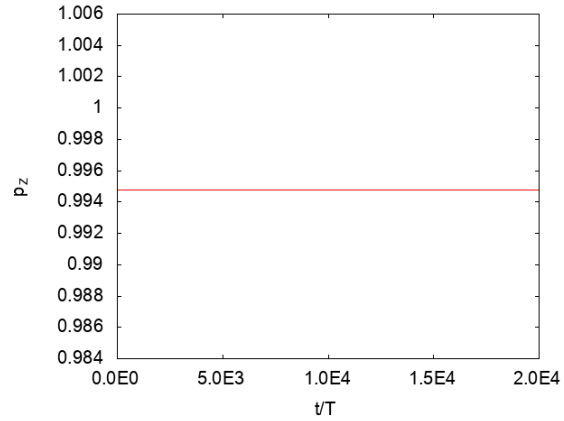

(d)

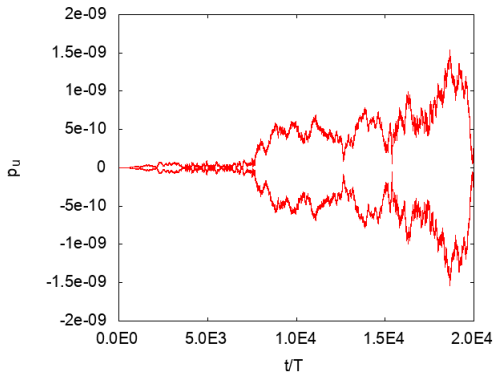

(e)

Figure 8: Midpoint rule applied to field configuration C1. (a) and (b) are the energy error respectively for the whole splitted flow and for a single part, (c) is the particle trajectory in the (x, y) plane, (d) and (e) are the z and u components of the discrete momentum (eq. 1.35)

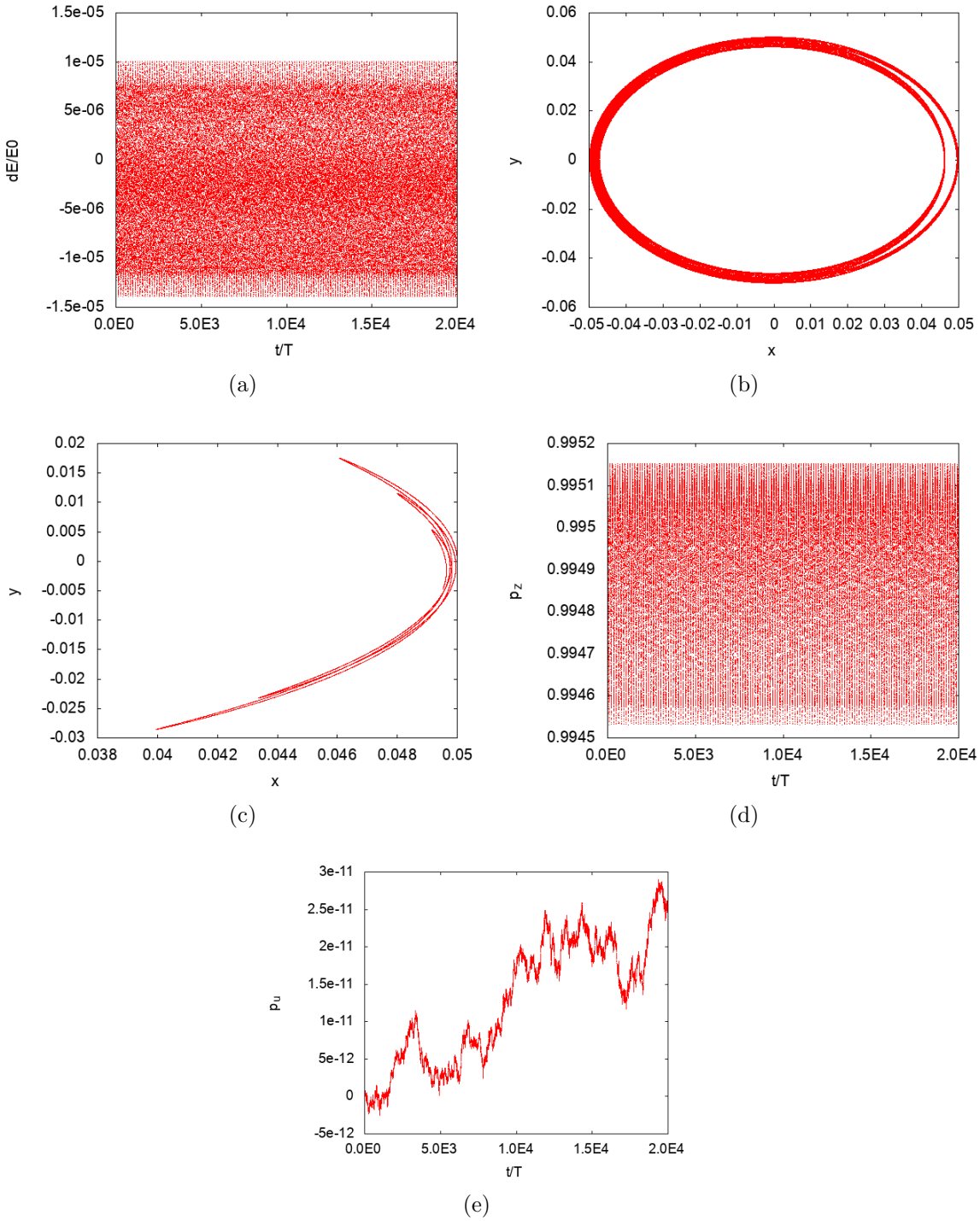

Figure 9: Midpoint rule applied to field configuration C2. (a) is the energy error, (b) is the particle trajectory in the (x, y) plane, (c) is a zoom showing the banana orbits, (d) and (e) are the z and u components of the discrete momentum (eq. 1.35)

1.4.2 Implicit Scheme 2: Three dimensional Lagrangian

We have already seen in chapter **??** that the continuous equations of motion can be solved trivially for u to give:

$$u = \hat{\mathbf{b}} \cdot \dot{\mathbf{x}} \tag{1.38}$$

It is quite easy to show that the Euler-Lagrange equations for the guiding center phase-space Lagrangian with the velocity u explicited with respect to the other variables are equivalent to the original Euler-Lagrange equations.
Thus, it is reasonable to wonder how a variational integrator would behave if applied to such Lagrangian:

$$\mathcal{L}(\mathbf{x}, \dot{\mathbf{x}}) = \mathbf{A}(\mathbf{x}) \cdot \dot{\mathbf{x}} + \frac{1}{2} \left(\mathbf{b}(\mathbf{x}) \cdot \dot{\mathbf{x}}\right)^2 - \mu B(\mathbf{x}) \tag{1.39}$$

The midpoint discretization gives:

$$\mathcal{L}_d(\mathbf{x}_0, \mathbf{x}_1) = \mathbf{A}(\tilde{\mathbf{x}}_0) \cdot \Delta\mathbf{x}_0 + \frac{1}{2h} \left(\mathbf{b}(\tilde{\mathbf{x}}_0) \cdot \Delta\mathbf{x}_0\right)^2 - h\mu B(\tilde{\mathbf{x}}_0) \tag{1.40}$$

The discrete integrator is then defined by matching of the discrete momenta:

$$\begin{aligned} \mathbf{p}_k &= \frac{\partial \mathcal{L}}{\partial \dot{\mathbf{x}}} \left(\tilde{\mathbf{x}_k}, \frac{\Delta\mathbf{x}_k}{2}\right) - \frac{h}{2} \frac{\partial \mathcal{L}}{\partial \mathbf{x}} \left(\tilde{\mathbf{x}_k}, \frac{\Delta\mathbf{x}_k}{2}\right) \\ \mathbf{p}_{k+1} &= \frac{\partial \mathcal{L}}{\partial \dot{\mathbf{x}}} \left(\tilde{\mathbf{x}_k}, \frac{\Delta\mathbf{x}_k}{2}\right) + \frac{h}{2} \frac{\partial \mathcal{L}}{\partial \mathbf{x}} \left(\tilde{\mathbf{x}_k}, \frac{\Delta\mathbf{x}_k}{2}\right) \end{aligned} \tag{1.41}$$

It is important to stress that this new Lagrangian is still degenerate (the degrees of freedom of the guiding center are two, hence a regular Lagrangian must be defined in a two dimensional space), and it doesn't correspond to a phase-space or an Hamiltonian formalism.
This is reflected to the fact that the Legendre transform is singular and new primary constraints arise. In fact, the Legendre transform reads:

$$\mathbf{p} \equiv \frac{\partial \mathcal{L}}{\partial \dot{\mathbf{x}}} = (\hat{\mathbf{b}} \cdot \dot{\mathbf{x}})\hat{\mathbf{b}} + \mathbf{A} \tag{1.42}$$

Hence, it is straightforward to show that there are two constraints:

$$\phi = \begin{pmatrix} A^x + \dfrac{b^x}{b^z}(p^z - A^z) - p^x \\ A^y + \dfrac{b^y}{b^z}(p^z - A^z) - p^y \end{pmatrix} \tag{1.43}$$

Also, from the Hamiltonian function of the original 4D system, we know that the following function H is conserved:

$$H = \frac{u^2}{2} + \mu B = \frac{(\hat{\mathbf{b}} \cdot \dot{\mathbf{x}})^2}{2} + \mu B = \frac{\|\mathbf{p} - \mathbf{A}\|^2}{2} + \mu B \tag{1.44}$$

This function is conserved along the orbits of the particle. However, it is important to stress that we can't just apply hamilton's equations to this function, as one could think, since the function H is identical in form to an Hamiltonian of a charged particle in an electromagnetic field.
In fact, the Lagrangian 1.39 does not possess an hamiltonian structure: it is neither a regular Lagrangian nor a phase-space Lagrangian. The only correct equations are the Euler-Lagrange equations for this Lagrangian, which are not the hamilton's equations for H.
These equations are again a set of implicit equations and have to be solved with a first guess integrator.
The procedure used is the following: we can map a point $(\mathbf{x}, \mathbf{p})$ to a 4D point $z = (\mathbf{x}, u)$ with the following equation:

$$u = \|\mathbf{p} - \mathbf{A}\| \tag{1.45}$$

Hence, we can find the velocity u_0 from a point $(\mathbf{x}_0, \mathbf{p}_0)$ of this 3D integrator, RK4 is applied to find the following point x_1, u_1 and finally Newton's method allows to converge to the implicit equations.
Alternatively, we can find the velocity u_0 from $\mathbf{x}_0$ and the 4D momenta p_0^z by imposing the 4D constraints (eq. 1.26). Finally, the point z_1, p_1^z is found with one of the linearizations explained afterwards and Newton iterations are used for converging the implicit equations.
We chose the latter method, since it gives the best results and it is the most performant.

Since all variables are velocity dependent, we expect that only the conjugate momenta relative to Noether symmetries are conserved.
Hence, field configurations A,B and C1 which are toroidally symmetric should conserve the z component of the discrete momentum:

$$p_k^z = \frac{\partial \mathcal{L}}{\partial \dot{z}} \left(\tilde{\mathbf{x}}_k, \frac{\Delta \mathbf{x}_k}{h} \right) = \frac{1}{h} (\hat{\tilde{\mathbf{b}}}_k \cdot \Delta \mathbf{x}_k) \tilde{b}_k^z + \tilde{A}_k^z = const. \tag{1.46}$$

Numerical Results Figure 10, 11, 12 and 13 show the numerical results respectively for the field configurations A,B, C1 and C2.
The toroidal conjugate momentum p^z is correctly conserved for the fields A,B and C1. Also, the energy is bounded for long times for all the cases in consideration.

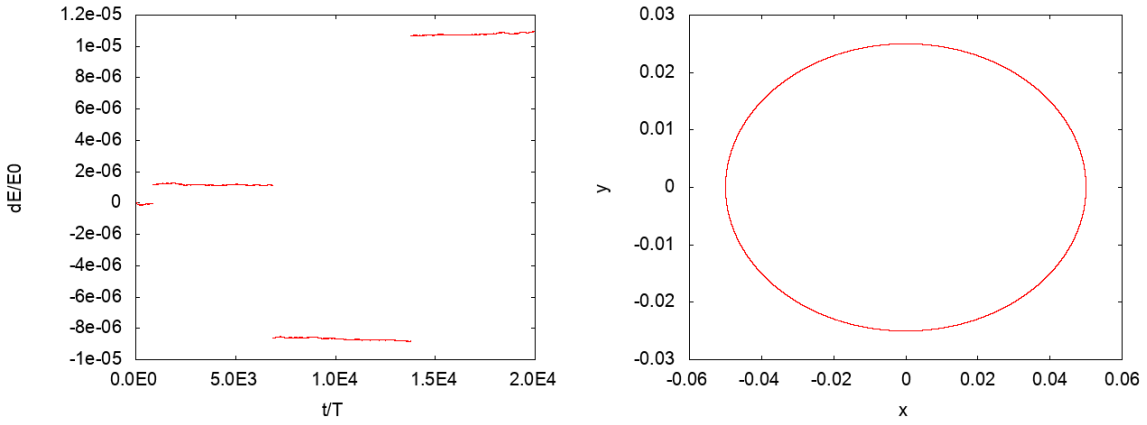

(a) (b)

(c) (d)

Figure 10: 3D Midpoint rule applied to field configuration A. (a) is the energy error, (b) is the particle trajectory in the (x, y) plane, (c) is the z component of the discrete momentum (eq. 1.46), (d) is the first component of the constraints (eq. 1.43)

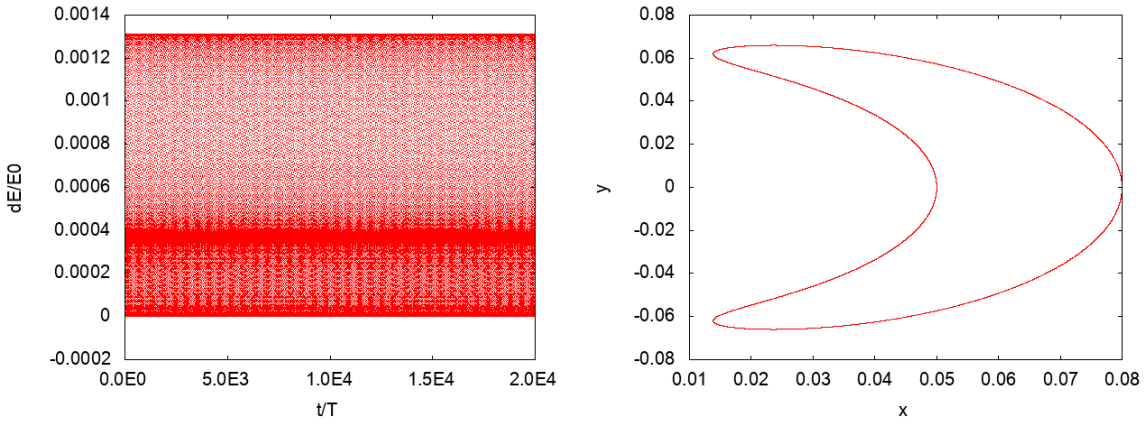

(a) (b)

(c) (d)

Figure 11: 3D Midpoint rule applied to field configuration B. (a) is the energy error, (b) is the particle trajectory in the (x,y)plane, (c) is the z component of the discrete momentum (eq. 1.46), (d) is the first component of the constraints (eq. 1.43)

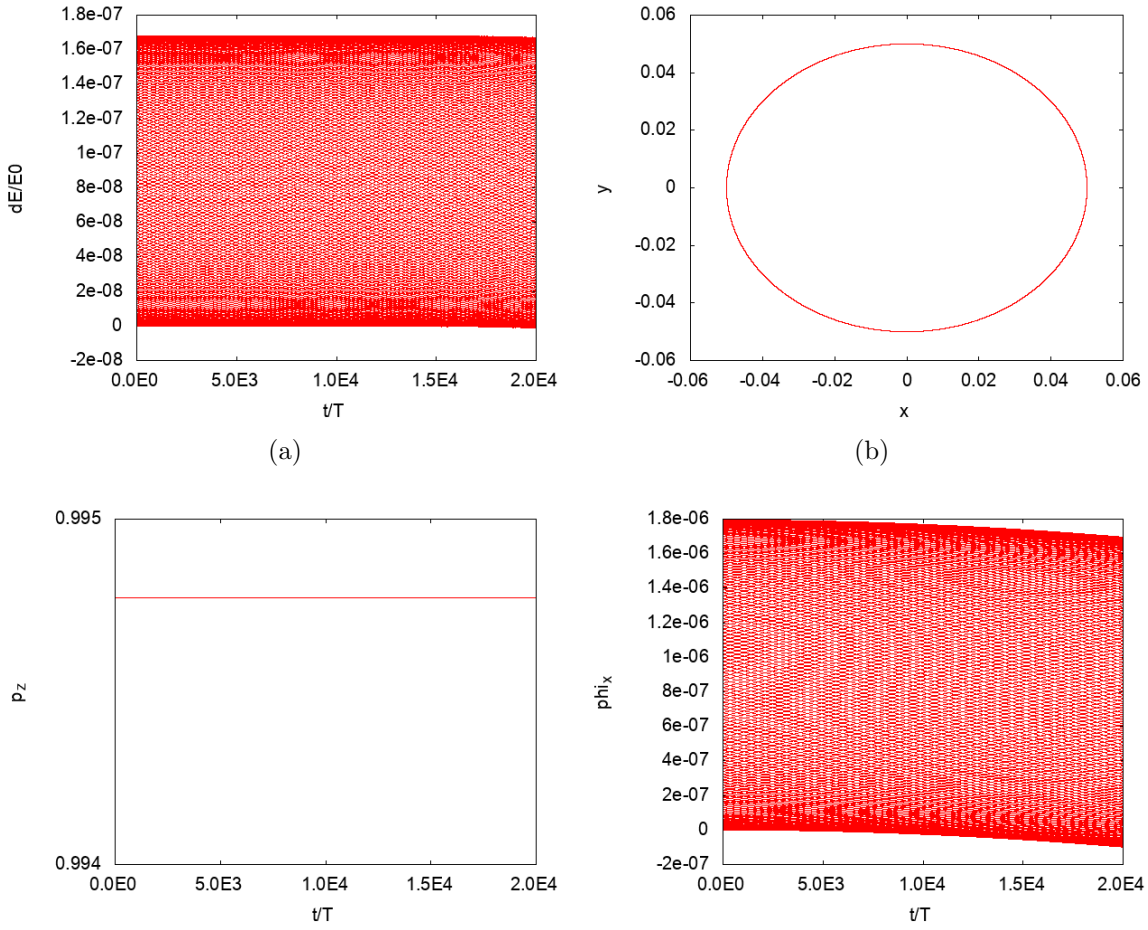

Figure 12: 3D Midpoint rule applied to field configuration C1. (a) is the energy error, (b) is the particle trajectory in the (x,y)plane, (c) is the z component of the discrete momentum (eq. 1.46), (d) is the first component of the constraints (eq. 1.43)

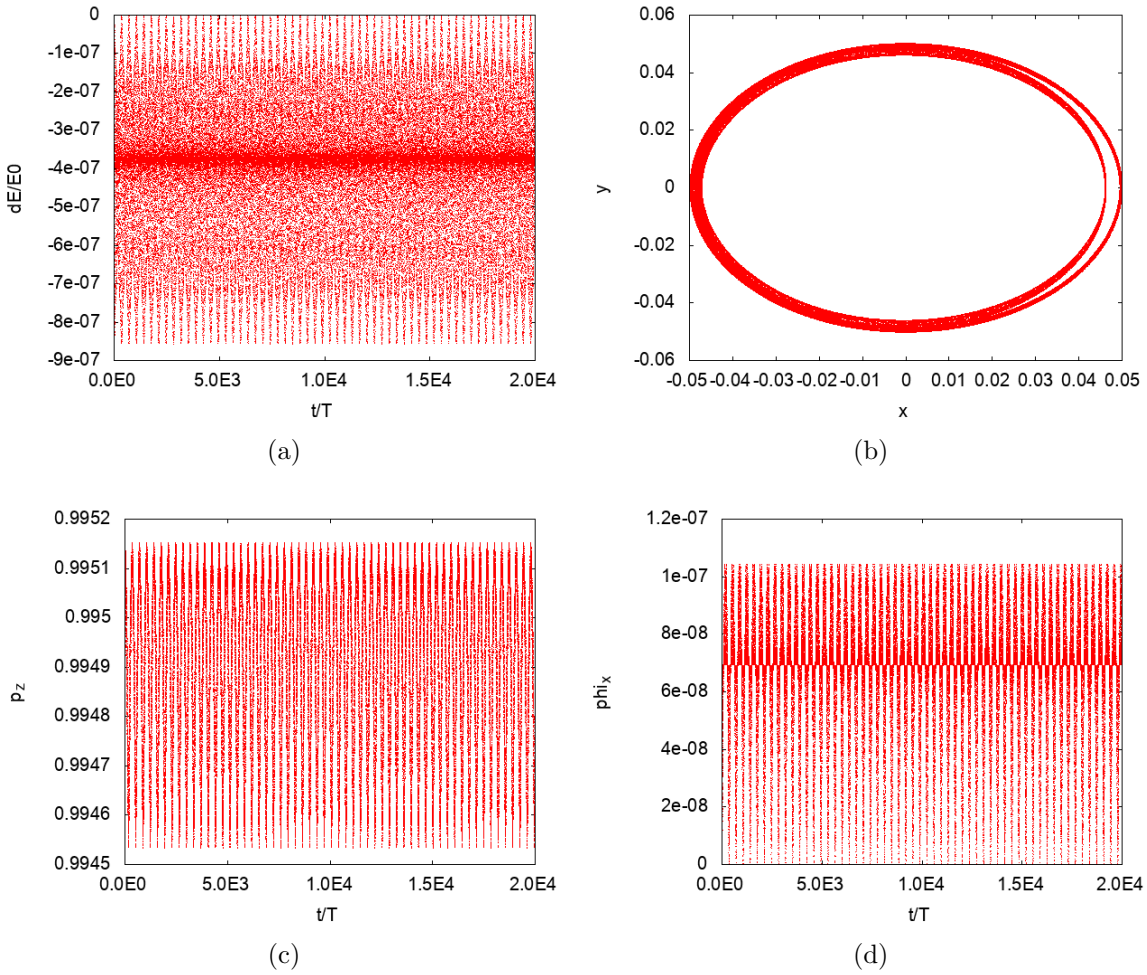

Figure 13: 3D Midpoint rule applied to field configuration C2b. (a) is the energy error, (b) is the particle trajectory in the (x,y)plane, (c) is the z component of the discrete momentum (eq. 1.46), (d) is the first component of the constraints (eq. 1.43)

1.4.3 Semiexplicit Scheme

In the original papers of Qin ([19] and [20]) a slightly different discrete Lagrangian was used, apparently for stability reasons and for other reasons that will be clear after the linearization done in the following paragraphs:

$$\mathcal{L}_d(\mathbf{z}_0, \mathbf{z}_1) = \frac{A_1^\dagger + A_0^\dagger}{2} \cdot \Delta x_0 - \frac{u_0 u_1}{2} - \mu B_0 \tag{1.47}$$

The main differences are the modified vector potential and the magnetic field evaluated exactly at each step rather than at the midpoint and the velocity term in the Hamiltonian.
We can notice that this has no longer a midpoint discretization form. Of course, the flow of the variational integrator applied to this modified Lagrangian is still symplectic and the discrepancy from the flow of the original midpoint Lagrangian is small.

Instabilities This integrator has shown to produce instabilites in all the magnetic field configuration we used. This behaviour is illustrated in figure 14, where a tokamak configuration was used. The instabilities are characterized by oscillations which are initially small and increase exponentially in times, breaking the integrator in a small amount of time and hence making it unusable in practice. Furthermore, they're present in some of the explicit schemes we will study below.
Squire and Qin [24] suggested that these instabilities could be due to an incorrect behaviour of the conserved sympelctic forms when the time step is brought to 0, and that they could be mitigated by searching for particular gauge transformations of the Lagrangian.

In the following paragraphs, we will suggest new explicit linearization of the symplectic integrator which are apparently free from instabilities.

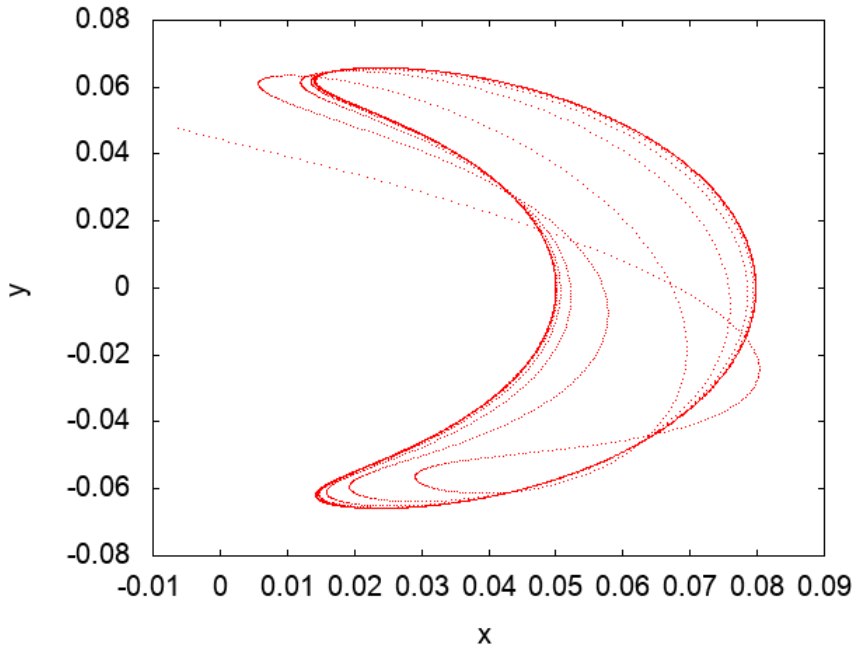

(a)

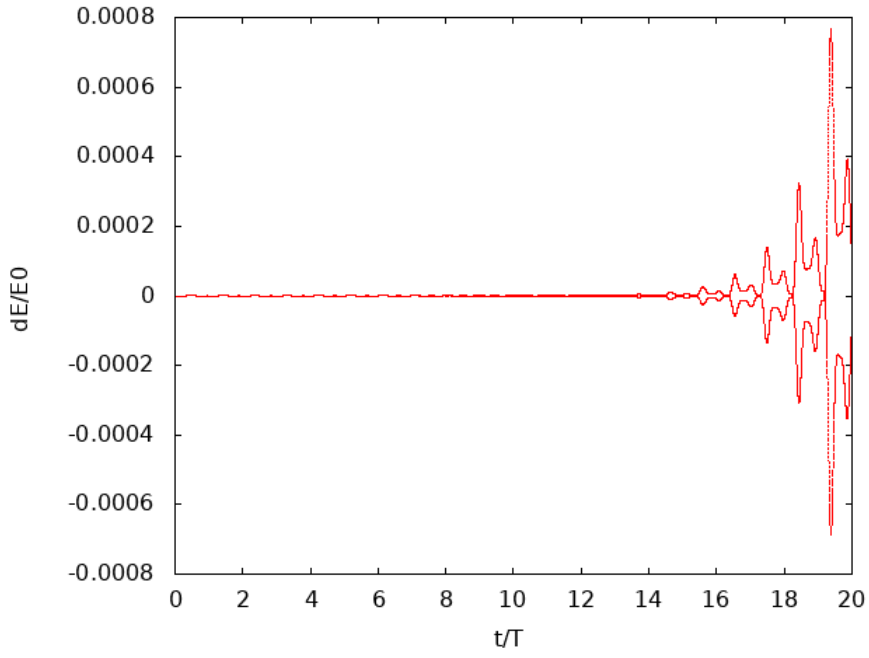

(b)

Figure 14: Instabilities produced by the linearized integrator with field configuration B. (a) is the particle trajectory in the poloidal plane (x, y), (b) is the energy error

1.4.4 Explicit Scheme 1

The purpose of this section is to find an explicit integrator which remains close to the solution. Of course, such an algorithm would be much faster than an implicit one. The standard technique is the linearization of the implicit scheme.

Let's start with equations (**??**):

$$\mathbf{p}_1 = \Theta(\tilde{\mathbf{z}}_1) + \frac{h}{2}\nabla H(\tilde{\mathbf{z}}_1) - \Theta^T_{(1)}(\tilde{\mathbf{z}}_1)\frac{\Delta \mathbf{z}_1}{2} \tag{1.48a}$$

$$= \Theta(\tilde{\mathbf{z}}_0) - \frac{h}{2}\nabla H(\tilde{\mathbf{z}}_0) + \Theta^T_{(1)}(\tilde{\mathbf{z}}_0)\frac{\Delta \mathbf{z}_0}{2} \tag{1.48b}$$

The idea of the linearization is to expand these equations around z_1, as we did in eqs (**??**) and to retain only the first two terms of the symplectic forms and the first term of the Hamiltonian:

$$\mathbf{p}_1 = \Theta_1 + \frac{h}{2}\nabla H_1 + \Omega_1\frac{\Delta \mathbf{z}_1}{2} \tag{1.49a}$$

$$= \Theta_1 - \frac{h}{2}\nabla H_1 - \Omega_1\frac{\Delta \mathbf{z}_0}{2} \tag{1.49b}$$

Hence, starting from two points $\mathbf{z}_0, \mathbf{p}_0$, we can find $\mathbf{z}_1$ and $\mathbf{p}_1$ with the following explicit equations:

$$\mathbf{z}_1 = \mathbf{z}_0 + 2\Omega_0^{-1}\left(\mathbf{p}_0 - \Theta_0 - \frac{h}{2}\begin{pmatrix} \mu\nabla B_0 \\ u_0 \end{pmatrix}\right) \tag{1.50}$$

$$\mathbf{p}_1 = \Theta_1 - \Omega_1\frac{\Delta \mathbf{z}_0}{2} - \frac{h}{2}\begin{pmatrix} \mu\nabla B_0 \\ u_0 \end{pmatrix} \tag{1.51}$$

Alternatively, subtracting eqs. (1.49), we can find the equations for $\mathbf{z}_2$ in Lagrangian form:

$$\frac{\Omega_1}{2}(\mathbf{z}_2 - \mathbf{z}_0) + h\begin{pmatrix} \mu\nabla B_1 \\ u_1 \end{pmatrix} = 0 \tag{1.52}$$

Following the same discussion done in the previous sections, we can notice that the integrator will still be splitted in two parts.
Again, the constraints will not be conserved as the symplectic form is not constant.

A legitimate question is what does happen if we choose to retain also the term linear in Δz in eq. (1.48). We will see in section 1.4.7 that this will have beneficial effects on the integrator.

For all of the linearizations we tried, the Lagrangian initialization performed much better than the Hamiltonian one, in contrast with the behaviour of the implicit integrators.
The Hamiltonian initialization proved to possess frequently drifts in the energy error and to be always imprecise. For this reason, we will use the Lagrangian initialization for all the linearized integrators.

Numerical Results Figure 15 shows the linearization applied to the 2D field A. The energy is bounded for long times and the momenta p_z and p_u are exactly conserved. The conservation of momenta in this case is just a fortunate coincidence and it is a consequence of the simplicity of the magnetic field considered.
All the other field configurations are unstable, similarly to the semiexplicit scheme.

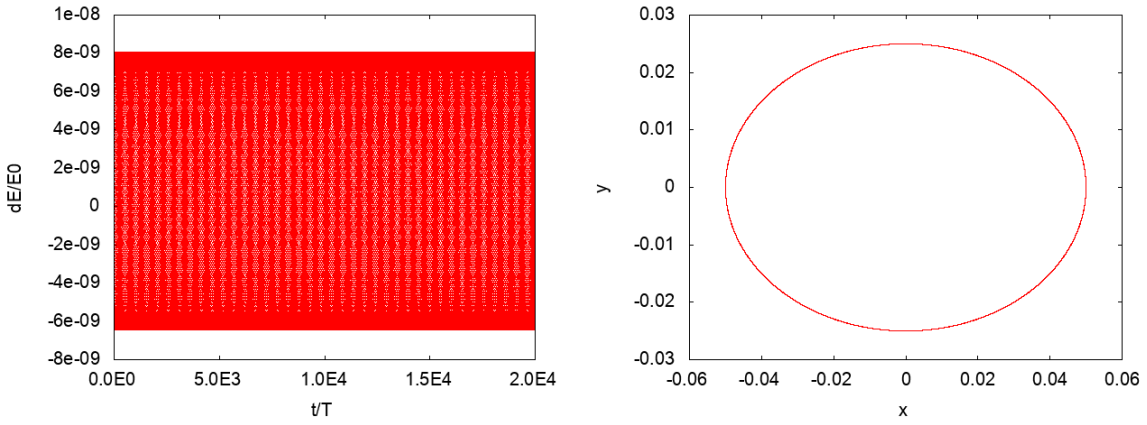

(a) (b)

(c) (d)

Figure 15: 3D Midpoint linearization applied to field configuration A. (a) is the energy error, (b) is the particle trajectory in the (x,y)plane, (c) is the z component of the discrete momentum (eq. 1.46), (d) is the u component of the discrete momentum

1.4.5 Explicit Scheme 2: Qin's Version

Starting from the semiexplicit Lagrangian (eq. 1.47), one can easily show that the linearization of all terms give rise to the same equations of the linearized midpoint Lagrangian with the exception of the quadratic velocity terms in the Hamiltonian. This modified velocity has proven to give better stability results than the original linearization.

The new discrete equations in position-momentum form take the following form:

$$\mathbf{p}_1 = \Theta_1 + \frac{h}{2}\nabla H_1 + \Omega_1^- \frac{\Delta \mathbf{z}_1}{2} \tag{1.53a}$$

$$= \Theta_1 - \frac{h}{2}\nabla H_1 - \Omega_1^+ \frac{\Delta \mathbf{z}_0}{2} \tag{1.53b}$$

where $\Omega^{\pm}$ are the following modified symplectic forms:

$$\Omega^{\pm} = \begin{pmatrix} 0 & -B_z^\dagger & B_y^\dagger & \hat{b}_x \\ B_z^\dagger & 0 & -B_x^\dagger & \hat{b}_y \\ -B_y^\dagger & B_x^\dagger & 0 & \hat{b}_z \\ -\hat{b}_x & -\hat{b}_y & -\hat{b}_z & \mp h \end{pmatrix} \tag{1.54}$$

The Lagrangian form reads:

$$\frac{\Omega_1^-}{2}(\mathbf{z}_2 - \mathbf{z}_1) + \frac{\Omega_1^+}{2}(\mathbf{z}_1 - \mathbf{z}_0) + h \begin{pmatrix} \mu \nabla B_1 \\ u_1 \end{pmatrix} = 0 \tag{1.55}$$

Writing explicitly the symplectic terms we get:

$$\begin{cases} \frac{1}{2}\left[A_1^{\dagger i,j} - A_1^{\dagger j,i}\right](x_2^i - x_0^i) - \frac{b_1^j}{2}\left[u_2 - u_0\right] = h\mu B_1^{,j} \\ \frac{1}{2} b_1^i (x_2^i - x_0^i) = \frac{h}{2}(u_2 + u_0) \end{cases} \tag{1.56}$$

Eventually, we can decouple the spatial part of the symplectic form from the velocity by substituting the velocity terms in the first three equations:

$$\begin{cases} \frac{1}{2}\left[A_1^{\dagger i,j} - A_1^{\dagger j,i}\right](x_2^i - x_0^i) - \frac{b_0^j}{2}\left[2u_0 - \frac{b_1^i}{h}(x_2^i - x_0^i)\right] = h\mu B_1^{,j} \\ \frac{1}{2} b_1^i (x_2^i - x_0^i) = \frac{h}{2}(u_2 + u_0) \end{cases} \tag{1.57}$$

so that the system can be solved by inverting a 3×3 matrix and by evaluating the velocity equation.

Numerical Results Similarly to the original linearization (section 1.4.4), the force-free configurations C1 and C2 are always unstable.
However, the region of instability of the tokamak field B is slightly smaller for this version and the instabilities proved to be very sensible to the initial conditions used.

Figure 16 and 17 show the results for the 2D field A and the tokamak field B with a Lagrangian initialization applied to the initial point

$$\mathbf{z}_0 = (\mathbf{x}_0, u_0) = (0.08461, 0.00228, 4.51147, -0.00057) \tag{1.58}$$

which proved to produce a stable flow.

The energy is bounded for both cases. Note that the z component of the momentum is no longer conserved, since the discrete Noether theorem is guaranteed to work only with the implicit symplectic integrator.

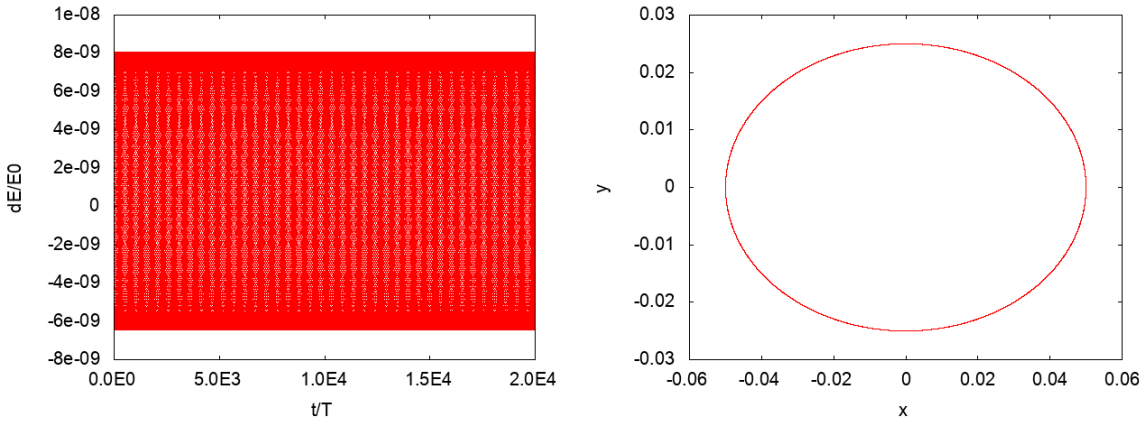

(a) (b)

(c) (d)

Figure 16: Qin linearization applied to field configuration A. (a) is the energy error, (b) is the particle trajectory in the (x,y)plane, (c) is the z component of the discrete momentum (eq. 1.46), (d) is the u component of the discrete momentum

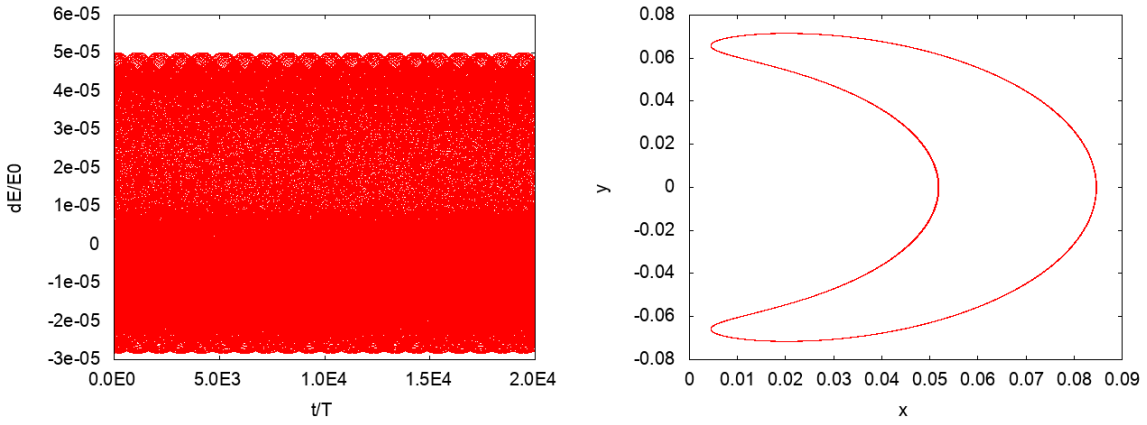

(a) (b)

(c) (d)

Figure 17: Qin linearization applied to field configuration B. (a) is the energy error, (b) is the particle trajectory in the (x,y)plane, (c) is the z component of the discrete momentum (eq. 1.46), (d) is the u component of the discrete momentum

1.4.6 Explicit Scheme 3

In the same spirit of section 1.4.2, we tried a different version of the linearization made by Qin.
The term $u_2 - u_0$ that appears in equations (1.57) is just the discretization of terms proportional to the derivative of u in the Taylor expansion of the one-form Θ.
This term was substituted by:

$$\frac{u_2 - u_0}{2h} \simeq \hat{b} \cdot \ddot{x} \simeq \frac{b_1^i (x_2^i - 2x_1^i + x_0^i)}{h^2} \tag{1.59}$$

This approximation seems quite rude; however, we will see that this integrator has some interesting properties.
Writing explicitly the discrete Euler-Lagrange equations, we get:

$$\begin{cases} \frac{1}{2}\left[A_1^{\dagger i,j} - A_1^{\dagger j,i}\right](x_2^i - x_0^i) - \frac{b_1^j b_1^i}{h}\left[x_2^i - 2x_1^i + x_0^i\right] = h\mu B_1^{\dagger j} \\ \frac{1}{2} b_1^i (x_2^i - x_0^i) = \frac{h}{2}(u_2 + u_0) \end{cases} \tag{1.60}$$

or equivalently in position-momentum form:

$$\mathbf{p}_1 = \Theta_1 + \frac{h}{2}\nabla H_1 + \Omega_1^- \frac{\Delta \mathbf{z}_1}{2} \tag{1.61a}$$

$$= \Theta_1 - \frac{h}{2}\nabla H_1 - \Omega_1^+ \frac{\Delta \mathbf{z}_0}{2} \tag{1.61b}$$

$$\Omega^{\pm} = \begin{pmatrix} 0 & -B_z^\dagger & B_y^\dagger & 0 \\ B_z^\dagger & 0 & -B_x^\dagger & 0 \\ -B_y^\dagger & B_x^\dagger & 0 & 0 \\ -\hat{b}_x & -\hat{b}_y & -\hat{b}_z & \mp h \end{pmatrix} \mp \frac{2 b^i b^j}{h} \tag{1.62}$$

Numerical Results Figure 18, 19, 20 and 21 show the numerical results for the configurations A,B,C1 and C2.
Unlike the previous cases, the integrator is stable for every configuration we tested. The energy is bounded for long times and the momenta p^z and p^u are conserved only in the 2D field configuration and bounded in the other cases.

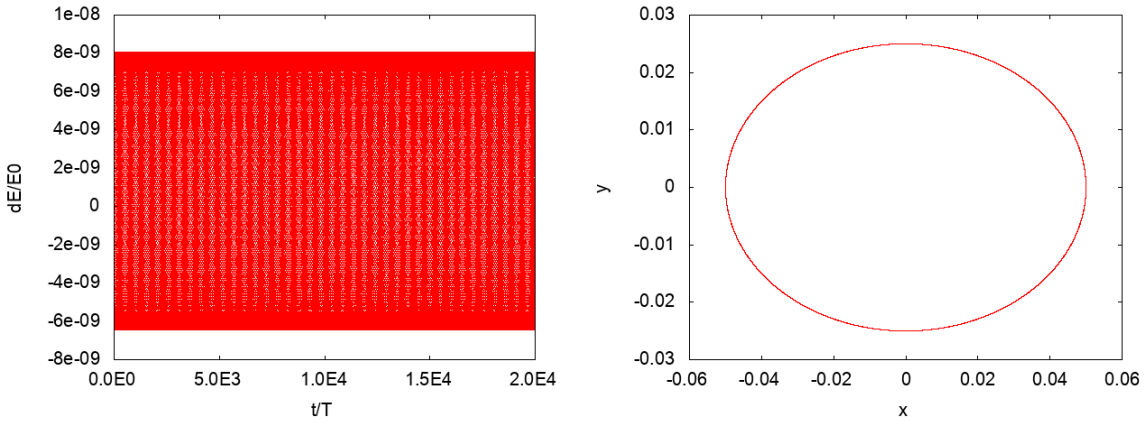

(a) (b)

(c) (d)

Figure 18: Modified Qin linearization applied to field configuration B. (a) is the energy error, (b) is the particle trajectory in the (x,y)plane, (c) is the z component of the discrete momentum (eq. 1.46), (d) is the u component of the discrete momentum

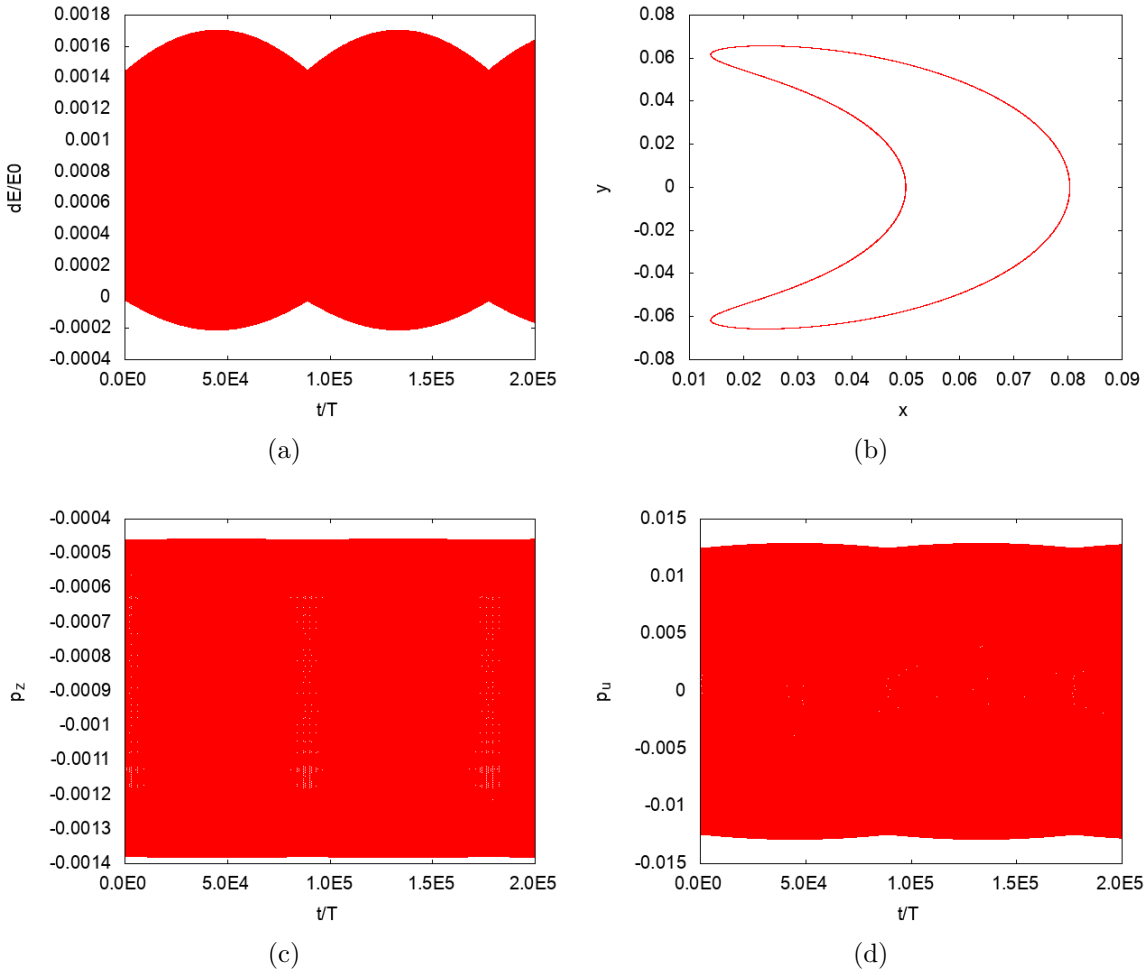

Figure 19: Modified Qin linearization applied to field configuration B. (a) is the energy error, (b) is the particle trajectory in the (x,y)plane, (c) is the z component of the discrete momentum (eq. 1.46), (d) is the u component of the discrete momentum

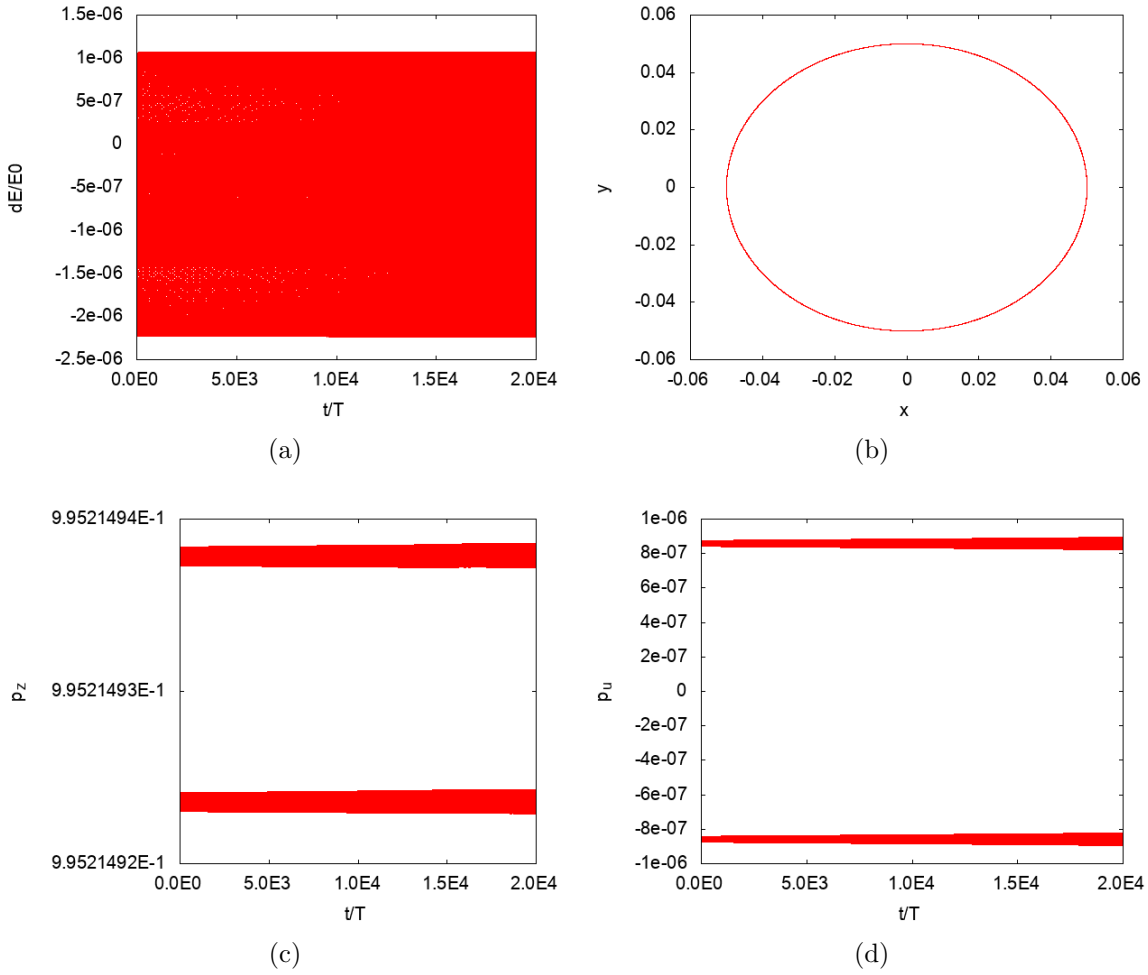

Figure 20: Modified Qin linearization applied to field configuration C1. (a) is the energy error, (b) is the particle trajectory in the (x,y)plane, (c) is the z component of the discrete momentum (eq. 1.46), (d) is the u component of the discrete momentum

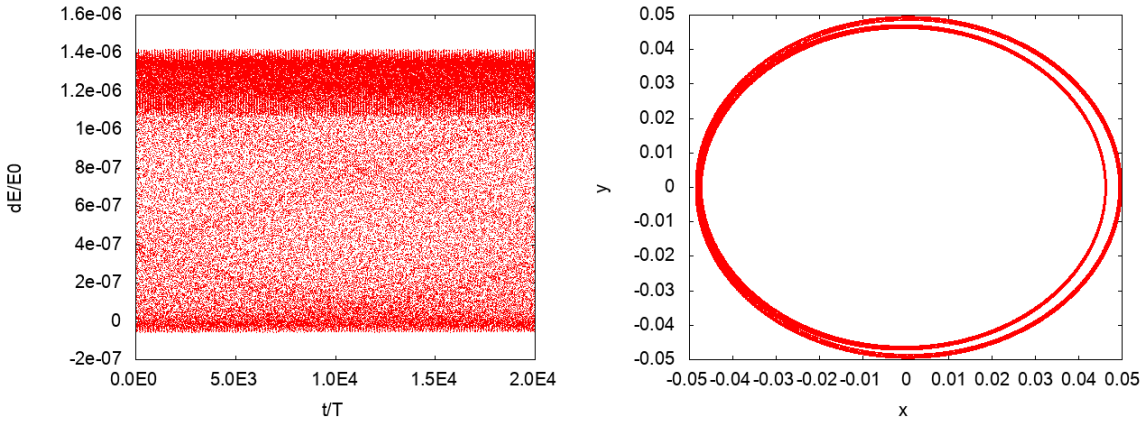

(a) (b)

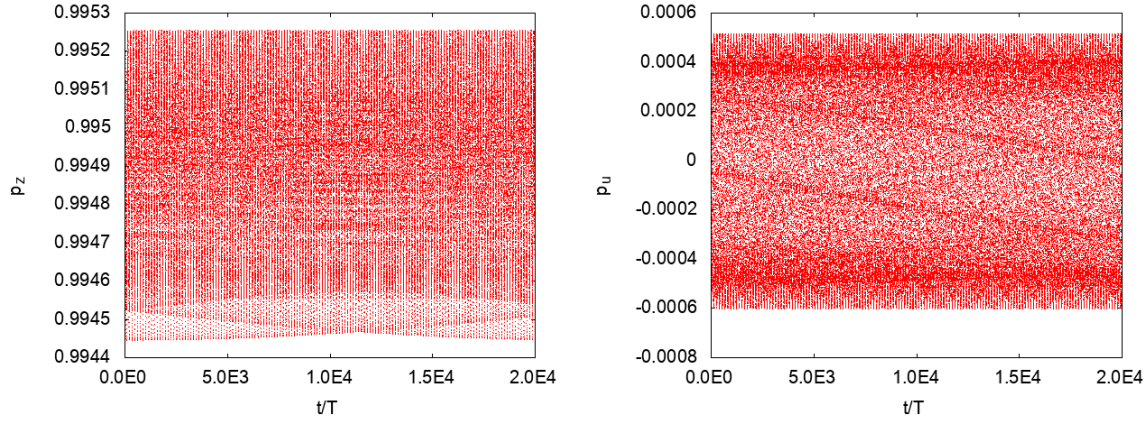

(c) (d)

Figure 21: Modified Qin linearization applied to field configuration C2b. (a) is the energy error, (b) is the particle trajectory in the (x,y)plane, (c) is the z component of the discrete momentum (eq. 1.46), (d) is the u component of the discrete momentum

1.4.7 Explicit Scheme 4: First order Hamiltonian

When we performed the truncation of the Taylor serie in equation 1.49, we chose to exclude the first order term of the Hamiltonian.
We can wonder how the linearization behave if we truncate the series to the first order, so that we can write:

$$\mathbf{p}_1 = \Theta_1 + \frac{h}{2}\nabla H_1 + \Omega_1 \frac{\Delta \mathbf{z}_1}{2} + \frac{h}{2}\nabla H_{1(1)} \frac{\Delta \mathbf{z}_1}{2} \tag{1.63a}$$

$$= \Theta_1 - \frac{h}{2}\nabla H_1 - \Omega_1 \frac{\Delta \mathbf{z}_0}{2} + \frac{h}{2}\nabla H_{1(1)} \frac{\Delta \mathbf{z}_0}{2} \tag{1.63b}$$

where $\nabla H_{1(1)}$ is the Hessian of the Hamiltonian. Matching the momenta we get:

$$\frac{\Omega_1}{2}(\mathbf{z}_2 - \mathbf{z}_0) + h \begin{pmatrix} \mu \nabla B_1 \\ u_1 \end{pmatrix} + \frac{h}{4} \begin{pmatrix} \mu B_{,i,j}(\mathbf{x}_1) & 0 \\ 0 & 1 \end{pmatrix} (\mathbf{z}_2 - 2\mathbf{z}_1 + \mathbf{z}_0) = 0 \tag{1.64}$$

As we will see shortly, the effect of these new terms is the removing of the instabilities typical of the original linearizations.

Dropping the magnetic terms We tried a sightly modified version by removing the second derivative of the magnetic field, so that eq. (1.64) is rewritten as:

$$\frac{\Omega_1}{2}(\mathbf{z}_2 - \mathbf{z}_0) + h \begin{pmatrix} \mu \nabla B_1 \\ u_1 \end{pmatrix} + \frac{h}{4} \begin{pmatrix} 0 & 0 \\ 0 & 1 \end{pmatrix} (\mathbf{z}_2 - 2\mathbf{z}_1 + \mathbf{z}_0) = 0 \tag{1.65}$$

The integrator thus found is almost unchanged. Computationally, this leads to a more effective algorithm, since the second derivative of the magnetic field could be expensive to compute, specially for the force-free configuration.

Numerical Results Figure 22, 23, 24 and 25 show the numerical results for the field A,B,C1 and C2.
The energy is bounded for all the configurations, the momenta p^z and p^u are only conserved for the 2D field and bounded for the other cases.
In all the tests we performed, no instabilities were observed.

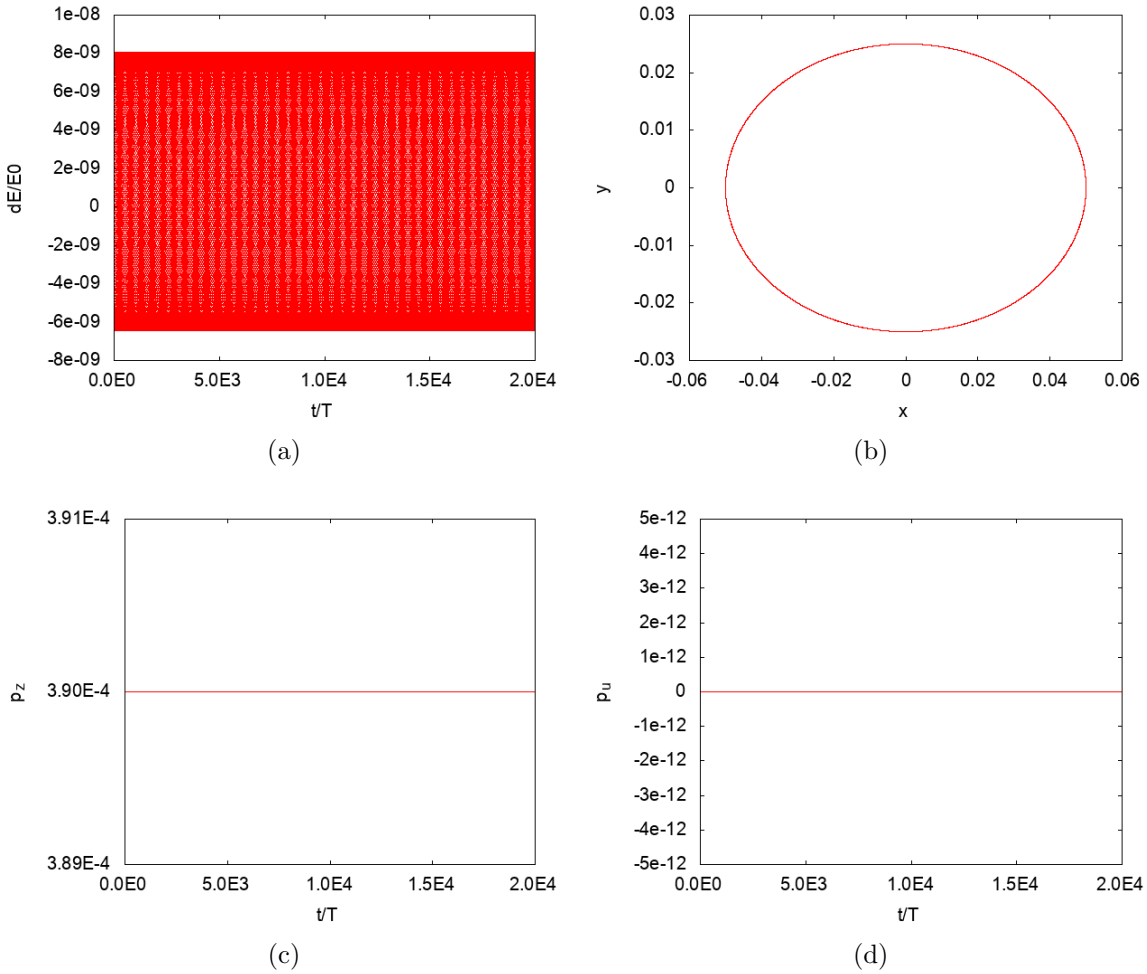

Figure 22: Linearization with first order Hamiltonian applied to field configuration A. (a) is the energy error, (b) is the particle trajectory in the (x,y)plane, (c) is the z component of the discrete momentum (eq. 1.46), (d) is the u component of the discrete momentum

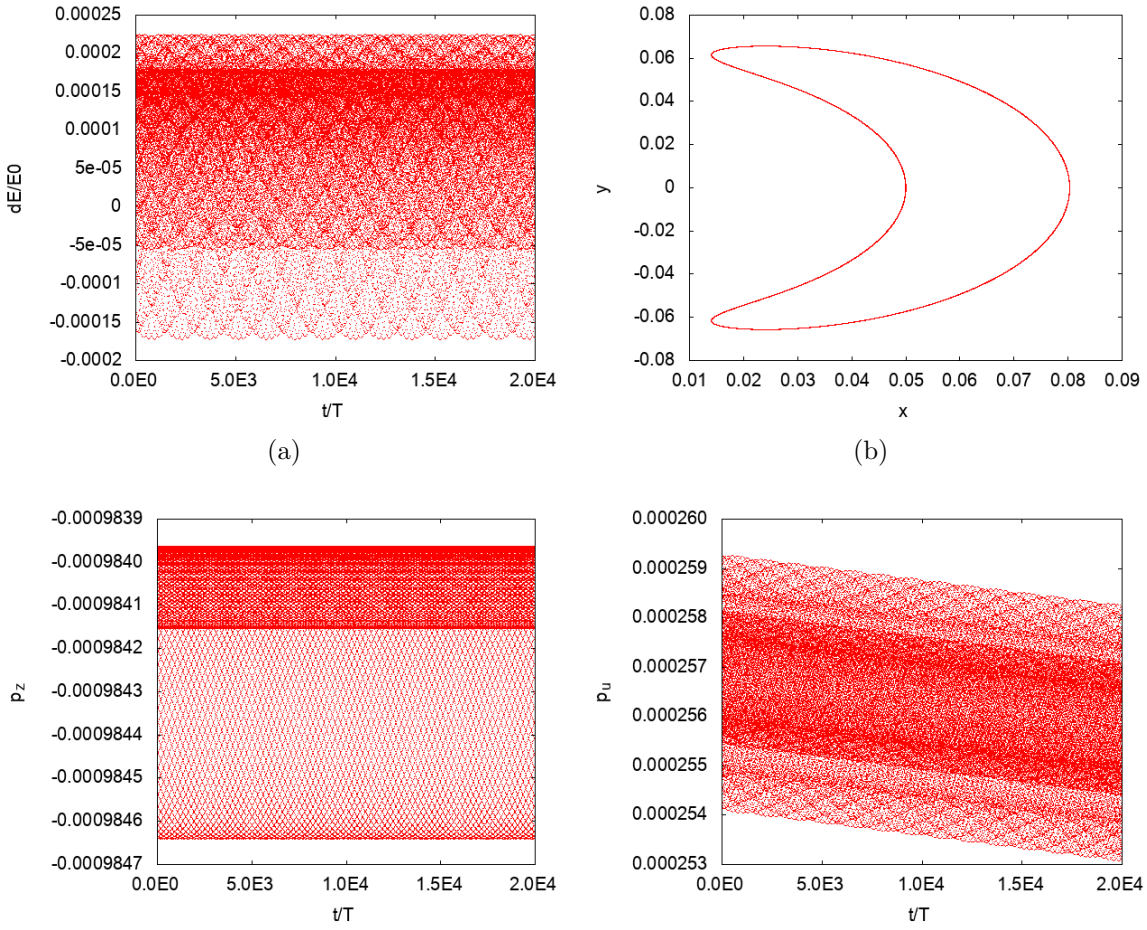

Figure 23: Linearization with first order Hamiltonian applied to field configuration B. (a) is the energy error, (b) is the particle trajectory in the (x,y)plane, (c) is the z component of the discrete momentum (eq. 1.46), (d) is the u component of the discrete momentum

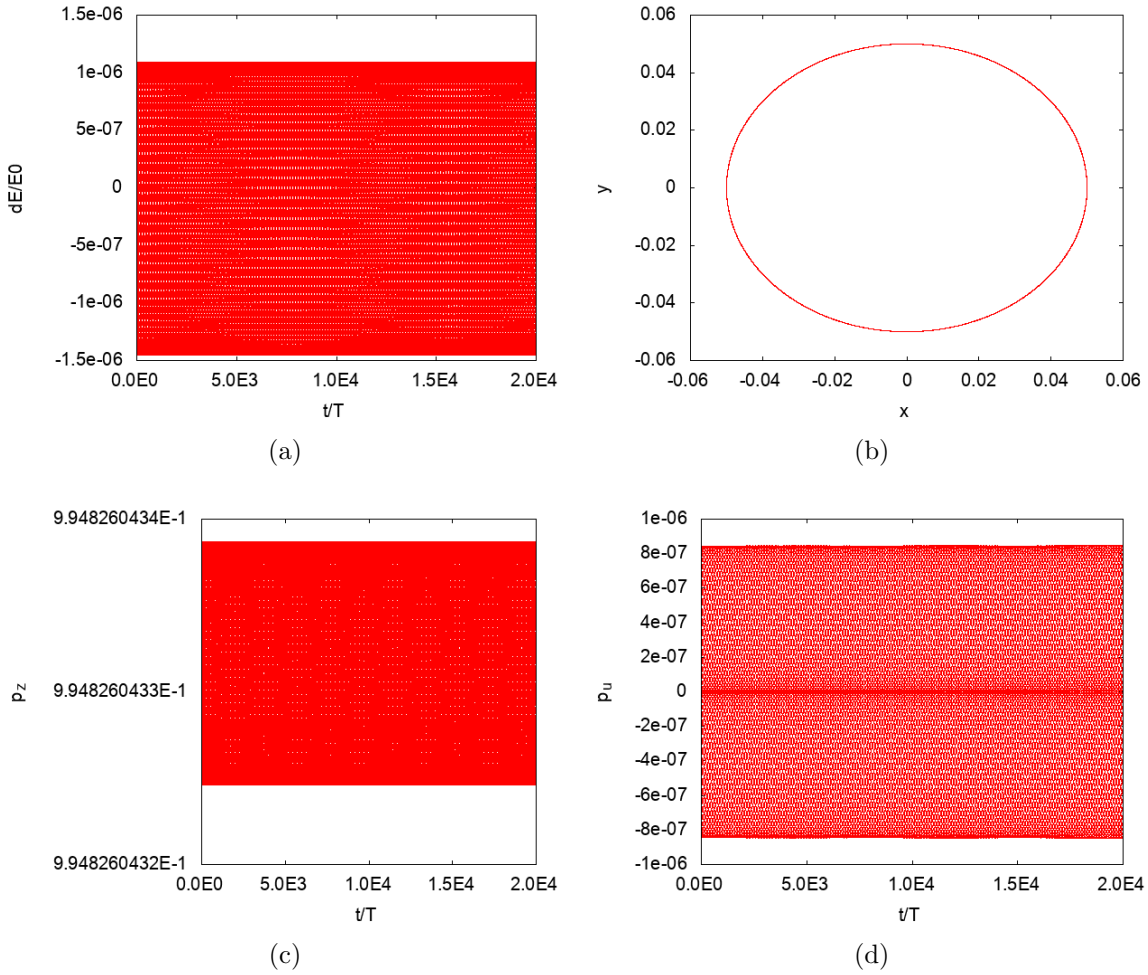

Figure 24: Linearization with first order Hamiltonian applied to field configuration C1. (a) is the energy error, (b) is the particle trajectory in the (x,y)plane, (c) is the z component of the discrete momentum (eq. 1.46), (d) is the u component of the discrete momentum

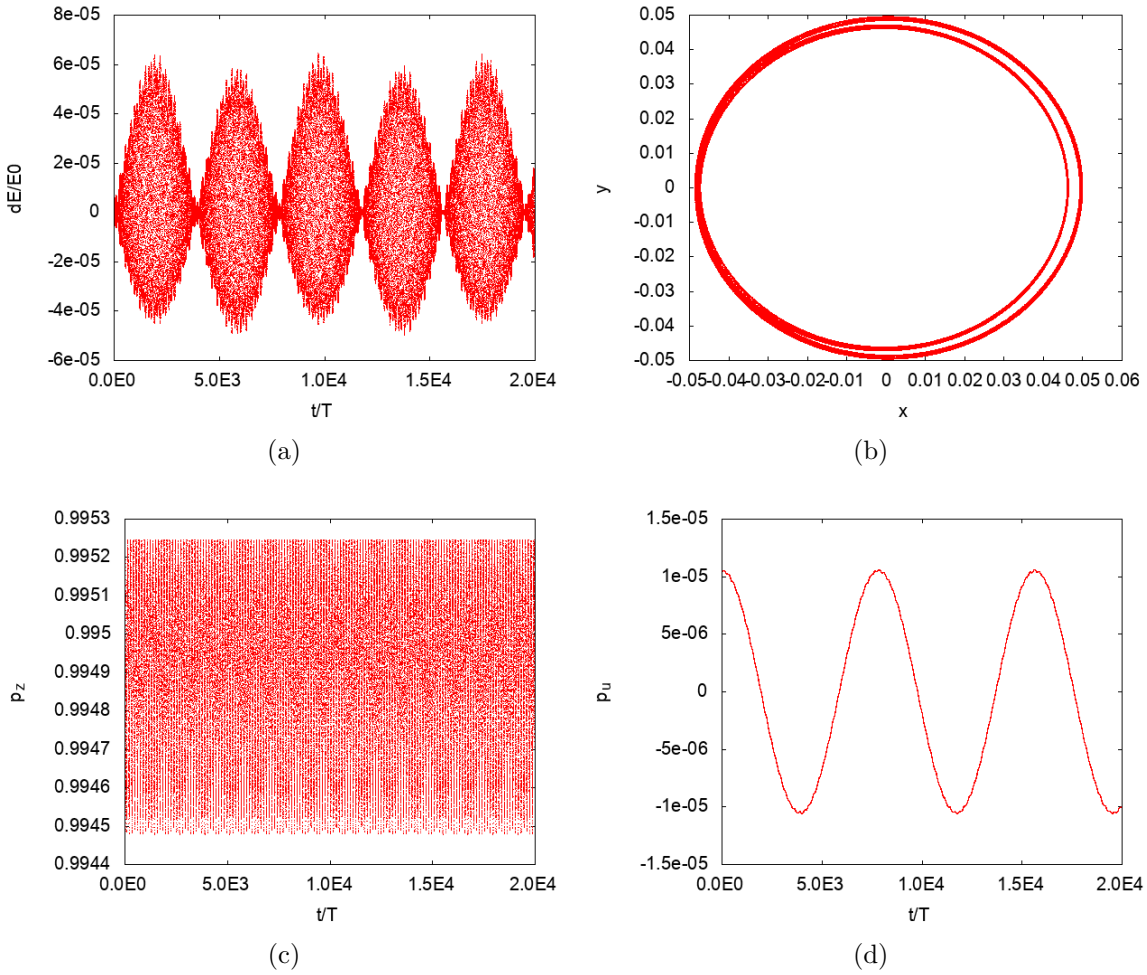

Figure 25: Linearization with first order Hamiltonian applied to field configuration C2. (a) is the energy error, (b) is the particle trajectory in the (x,y)plane, (c) is the z component of the discrete momentum (eq. 1.46), (d) is the u component of the discrete momentum

1.5 Review and comparison with RK4

Figure 27 shows the energy error for the field configuration B plotted as a function of time for the fourth order Runge-Kutta, the implicit scheme 1 and the explicit scheme 4.
In the case of RK4, the energy quickly decays, showing the inefficiency of this integrator for high time steps and high integration times.
All the symplectic integrators bounds the energy for long times, with the exception of the midpoint rule applied to the force-free configuration C1, which presents a small energy drift. The reason of this behaviour is unknown.
Note that the linearizations studied in this thesis has the same, and sometimes even better, accuracy than the non linearized midpoint rule.

The quantities associated to Noether symmetries are exactly conserved only with the non linearized integrators, both the 4D (section 1.4.1) and the 3D version (section 1.4.2). In the explicit versions, the Noether quantities are not exactly conserved, but still bounded.

It is worth noticing that all the implicit integrators require an Hamiltonian initialization, since the Lagrangian initialization produces very high drifts in the energy error.
This behaviour is the opposite for the linearized versions, which require a Lagrangian initialization to work correctly.
The complete comprehension of the theoretical aspects of this subject is very important and could lead to a better choice of the initialization.

The following table summarizes all these properties.

Integrator	Section	Error Bounding	Noether	Stability	Initialization
RK4		No	No	**Yes**	-
Implicit 1	1.4.1	**Yes** (for A,B,C2)	**Yes**	**Yes**	Hamiltonian
Implicit 2	1.4.2	**Yes**	**Yes**	**Yes**	Hamiltonian
Semiexplicit	1.4.3	**Yes**	**Yes**	No	Hamiltonian
Explicit 1	1.4.4	**Yes**	No	No	Lagrangian
Explicit 2	1.4.5	**Yes**	No	No	Lagrangian
Explicit 3	1.4.6	**Yes**	No	**Yes**	Lagrangian
Explicit 4	1.4.7	**Yes**	No	**Yes**	Lagrangian

Table 1: Comparison between the numerical integrators used in this chapter for the error bounding (see section **??**), the conservation of Noether quantities (section **??**), stability (section 1.4.3) and the correct initialization (section 1.3)

1.6 Stability Analysis

The explicit scheme 1 (section 1.4.4) and the Qin's version (section 1.4.5) are usually unstable and thus unusable in many cases.
However, we have found two linearizations, the explicit scheme 3 (section 1.4.6) and 4 (1.4.7) which are apparently free from instabilities, at least with the cases we studied.

One way to show the stability properties of these integrators is by studying the **Lyapunov exponents**. Usually, the Lyapunov exponents are used to study the rate of separation of infinitesimally close trajectory of a dynamical system.

Specifically, if the starting points of two trajectories are separated by a small quantity δx_0, the separation of the trajectories evolves approximately as:

$$|\delta x(t)| \simeq e^{\lambda t}|\delta x_0| \tag{1.66}$$

where λ is the Lyapunov exponent. For a discrete multidimensional system, it can be shown [**?**] that the whole spectrum of Lyapunov exponents can be found with:

$$\lambda_i(\mathbf{z}_0) = lim_{k\to\infty}\frac{1}{2k}\ln|\mu_i\left(\Phi_k^T\Phi_k\right)| \tag{1.67}$$

where Φ_k is the product of the jacobians of the discrete flow from the initial point to the time step k:

$$\Phi_k = F'(\mathbf{z}_k)\cdots F'(\mathbf{z}_0) \tag{1.68}$$

and μ_i denotes the i-th eigenvalue.

The maximum value of the Lyapunov exponents, called the **maximal Lyapunov exponent** (MLE), is useful to study the stability or the chaotic behaviour of a

system. In particular, if the MLE is negative or zero, the system is stable, and it is conservative if the MLE is zero. A positive MLE is an indication of a chaotic system, where two initial nearby points will diverge to an arbitrary separation, no matter how close they are.

Numerical results The Lyapunov exponents of the stable versions of our integrator have been analyzed with the above method with different initial conditions, and all of them have proved to be Lyapunov stable. Figure 26 shows the MLE for the tokamak configuration B, tested with the explicit scheme 4.

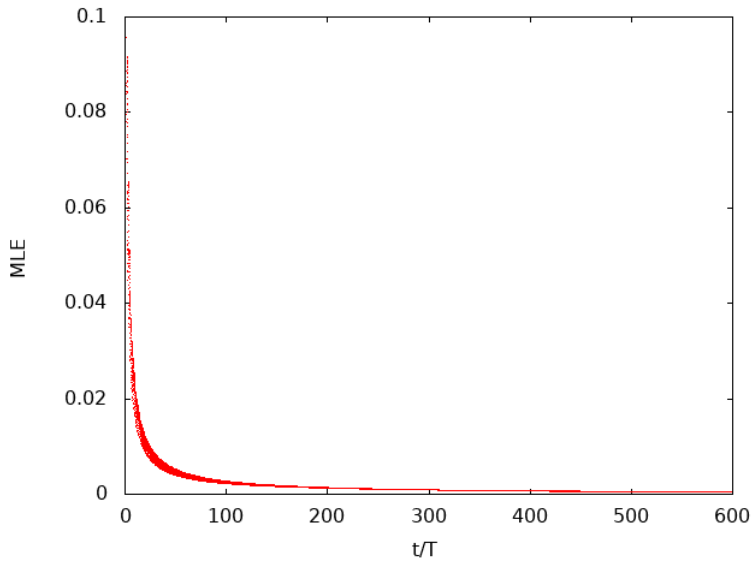

Figure 26: Maximal Lyapunov Exponent for the Explicit Scheme 4 (Section 1.4.7) and magnetic configuration B.

1.7 Computational Costs

Since the implicit integrators require generally two to four Newton iterations for the convergence plus an explicit first guess and one iteration requires one evaluation of the magnetic fields, we expect that these integrators should be slightly more costly, but still comparable, to RK4, which requires four field evalutions.
In particular, the 3D version of the midpoint rule should be slightly faster than the 4D version since we have one less degree of freedom.
The explicit integrators are the most efficient ones. By comparing eqs. (1.52) and (1.4), we recognize at once that an explicit integrator is equivalent to an Euler

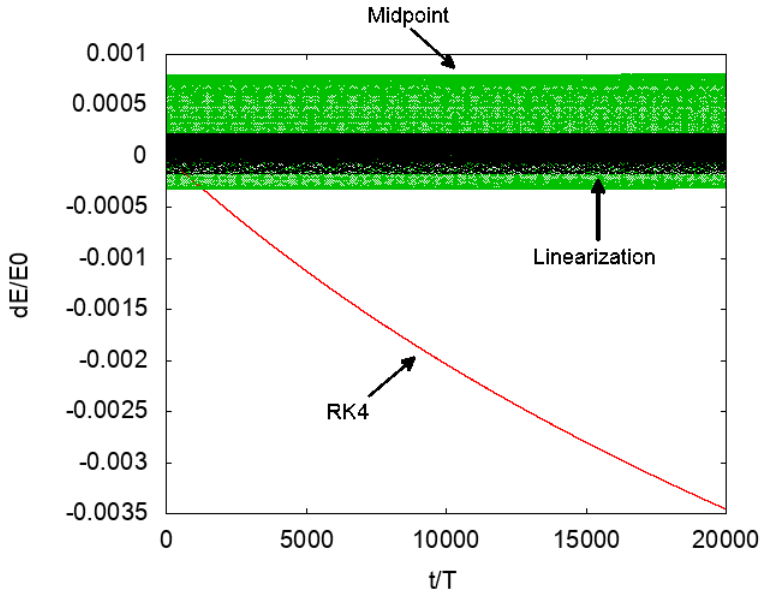

(a)

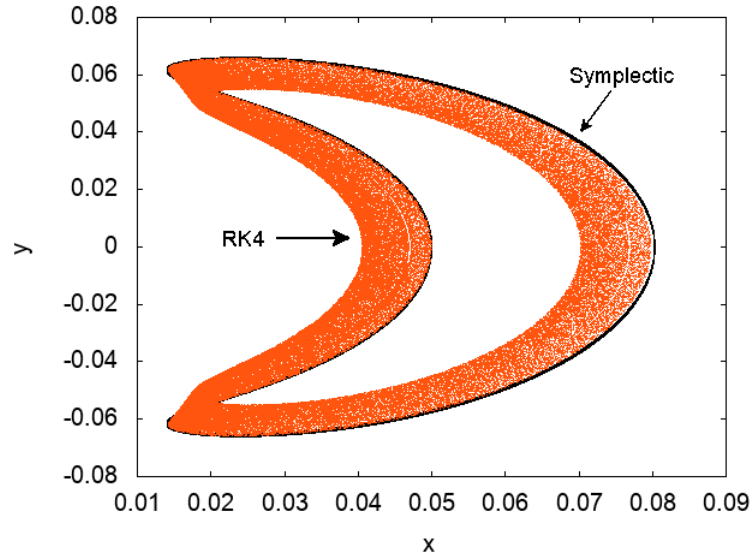

(b)

Figure 27: Comparison between RK4 and the variational symplectic integrators for the tokamak field configuration B. (a) is the energy error, (b) is the particle trajectory in the poloidal (x,y) plane.

method. A typical simulation of a tokamak like magnetic field for 2×10^4 orbits was

performed by the integrator in about 10 to 20 seconds in an old notebook.

References

[1] Giancarlo Benettin and Antonio Giorgilli. On the hamiltonian interpolation of near-to-the identity symplectic mappings with application to symplectic integration algorithms. *Journal of Statistical Physics*, 74(5-6):1117–1143, 1994.

[2] Peter G. Bergmann. Hamilton-jacobi theory with mixed constraints. *Transactions of the New York Academy of Sciences*, 33(1 Series II):108–115, 1971.

[3] James A. Cadzow. Discrete calculus of variations. *International Journal of Control*, 11(3):393–407, 1970.

[4] J. R. Cary and A. J. Brizard. Hamiltonian theory of guiding-center motion. *Reviews of Modern Physics*, 81(3):693–738, 2009.

[5] S. Chandrasekhar. On force-free magnetic fields. *Proceedings of the National Academy of Sciences of the United States of America*, 42(1):1–5, 1956.

[6] M. de León, J. C. Marrero, D. M. de Diego, and M. Vaquero. On the Hamilton-Jacobi theory for singular lagrangian systems. *Journal of Mathematical Physics*, 54(3):032902, 2013.

[7] R. de Vogelaere. Methods of integration which preserve the contact transformation property of the hamiltonian equations. *Report No. 4, Dept. Math., Univ. of Notre Dame, Notre Dame*, 1956.

[8] E. Forest and R. D. Ruth. Fourth-order symplectic integration. *Phys. D*, 43(1):105–117, 1990.

[9] H. Goldstein, C.P. Poole, and J.L. Safko. *Classical Mechanics, 3e.* Addison-Wesley Longman, Incorporated, 2002.

[10] Ernst Hairer. Backward analysis of numerical integrators and symplectic methods. In *Stiff and Differential-Algebraic Problems*. Springer-Verlag, 1994.

[11] Ernst Hairer, Christian Lubich, and Gerhard Wanner. *Geometric numerical integration*, volume 31. Springer, 2003.

[12] Sameer M Jalnapurkar, Melvin Leok, Jerrold E Marsden, and Matthew West. Discrete routh reduction. *Journal of Physics A: Mathematical and General*, 39(19):5521, 2006.

[13] B. Karasözen. Poisson integrators. *Mathematical and Computer Modelling*, 40(1112):1225–1244, 2004.

[14] S Lall and M West. Discrete variational hamiltonian mechanics. *Journal of Physics A: Mathematical and General*, 39(19):5509, 2006.

[15] Paulette Libermann and Charles-Michel Marle. *Symplectic geometry and analytical mechanics*, volume 35. Springer, 1987.

[16] Robert G. Littlejohn. Variational principles of guiding centre motion. *Journal of Plasma Physics*, 29(1):111–125, 1983.

[17] Jerrold E Marsden and Tudor S Ratiu. *Introduction to mechanics and symmetry: a basic exposition of classical mechanical systems*, volume 17. Springer, 1999.

[18] Jerrold E Marsden and Matthew West. Discrete mechanics and variational integrators. *Acta Numerica*, 10:357–514, 2001.

[19] Hong Qin and Xiaoyin Guan. Variational symplectic integrator for long-time simulations of the guiding-center motion of charged particles in general magnetic fields. *Physical review letters*, 100(3):035006, 2008.

[20] Hong Qin, Xiaoyin Guan, and William M Tang. Variational symplectic algorithm for guiding center dynamics and its application in tokamak geometry. *Physics of Plasmas*, 16(4):042510, 2009.

[21] Sebastian Reich. Backward error analysis for numerical integrators. *SIAM Journal on Numerical Analysis*, 36(5):1549–1570, 1996.

[22] Clarence W Rowley and Jerrold E Marsden. Variational integrators for degenerate lagrangians, with application to point vortices. In *Decision and Control, 2002, Proceedings of the 41st IEEE Conference on*, volume 2, pages 1521–1527. IEEE, 2002.

[23] R. D. Ruth. A Canonical Integration Technique. *IEEE Transactions on Nuclear Science*, 30(4):2669, 1983.

[24] J. Squire, H. Qin, and W. M. Tang. Gauge properties of the guiding center variational symplectic integrator. *Physics of Plasmas*, 19(5):052501, 2012.

[25] Namikawa T. Magneto-hydrodynamic oscillations of a conducting liquid mass rotating in a uniform magnetic field. *Journal of Geomagnetism and Geoelectricity*, 7(4):97, 1955.